

Leading twist nuclear shadowing: uncertainties, comparison to experiments and higher twist effects

L. Frankfurt

*Nuclear Physics Dept., School of Physics and Astronomy,
Tel Aviv University, 69978 Tel Aviv, Israel**

V. Guzey

*Institut für Theoretische Physik II,
Ruhr-Universität Bochum, D-44780 Bochum, Germany†*

M. Strikman

Department of Physics, the Pennsylvania State University, State College, PA 16802, USA‡

Abstract

Using the leading twist approach to nuclear shadowing, which is based on the relationship between nuclear shadowing and diffraction on a nucleon, we calculate next-to-leading order nuclear parton distribution functions (nPDFs) and structure functions in the region $0.2 > x > 10^{-5}$ and $Q^2 \geq 4 \text{ GeV}^2$. The uncertainties of our predictions due to the uncertainties of the experimental input and the theory are quantified. We determine the relative role of the small ($\sim Q^2$) and large ($\gg Q^2$) diffractive masses in nuclear shadowing as a function of x and find that the large mass contribution, which is an analog of the triple Pomeron exchange, becomes significant only for $x \leq 10^{-4}$. Comparing our predictions to the available fixed-target nuclear DIS data, we argue, based on the current experimental studies of the leading twist diffraction, that the data at moderately small $x \sim 0.01$ and $Q^2 \sim 2 \text{ GeV}^2$ could contain significant higher twist effects hindering the extraction of nPDFs from that data. Also, we find that the next-to-leading order effects in nuclear shadowing in the ratio of the nucleus to nucleon structure functions F_2 are quite sizable. Within the same formalism, we also present results for the impact parameter dependence of nPDFs. We also address the problem of extracting of the neutron $F_{2n}(x, Q^2)$ from the deuteron and proton data. We suggest a simple and nearly model-independent procedure of correcting for nuclear shadowing effects using F_2^A/F_2^D ratios.

PACS numbers: 24.85.+p,13.60.Hb

*frankfur@lev.tau.ac.il

†vadim.guzey@tp2.ruhr-uni-bochum.de

‡strikman@phys.psu.edu

I. INTRODUCTION

One way to analyze the microscopic structure of atomic nuclei is to study the distribution of quarks and gluons, as well as their correlations, in nuclei. These nuclear parton distribution functions (nPDFs) can be accessed using various deep inelastic scattering (DIS) processes: Inclusive scattering of leptons, high-mass dimuon production using proton beams, exclusive electroproduction of vector mesons. None of the above processes determines nPDFs comprehensively, only taken together do these experiments provide stringent constraints on nPDFs.

The discussion of the present paper is centered around the nuclear effects of nuclear shadowing and antishadowing (enhancement), which affect nPDFs at small values of Bjorken variable x , $10^{-5} \leq x \leq 0.2$. Nuclear shadowing of nPDFs is developing into an increasingly important subject because it is involved in the interpretation of the RHIC data on jet production, evaluation of hard phenomena in proton-nucleus and nucleus-nucleus collisions at the LHC, estimates of the black limit scattering regime in DIS, etc.

The major obstacle that hinders our deeper knowledge of nPDFs at small x is that, up to the present day, all experiments aiming to study nPDFs are performed with fixed (stationary) nuclear targets. In these data, the values of x and Q^2 are strongly correlated and one measures nPDFs essentially along a curve in the $x - Q^2$ plane rather than exploring the entire plane. Moreover, for $Q^2 > 1 \text{ GeV}^2$, the data cover the region $x > 5 \times 10^{-3}$, where the effect of nuclear shadowing is just setting in. As a result, when one attempts to globally fit the available data by modeling nPDFs at some initial scale Q_0^2 and then performing QCD evolution, various groups [1, 2, 3, 4, 5] produce significantly different results.

An alternative to the fitting to the data is to combine the Gribov theory [6], which relates the nuclear shadowing correction to the total hadron-deuteron cross section to the cross section of diffraction off a free nucleon, with the Collins factorization theorem [7] for hard diffraction in DIS. The resulting leading twist theory of nuclear shadowing was developed in [8] and later elaborated on in [9].

The Gribov theory has been applied to the description of nuclear shadowing for many years. First it was done in the region of small Q^2 , where generalized vector dominance model gives a good description of diffraction, see review in [10], and later in deep inelastic region, where large diffractive masses $M^2 \propto Q^2$ dominate [11]. A number of successful model

calculations were performed [12, 13, 14, 15, 16, 17, 18, 19, 20] before the experimental data from HERA became available. A calculation constrained to reproduce the HERA data using the Gribov theory was presented in [21]. It focuses on the calculation of nuclear shadowing for F_2^A at intermediate Q^2 where leading and higher twist effects are equally important. A fair agreement of the data with the Gribov theory has been found. However, this approach does not involve the use of the Collins factorization theorem and, hence, does not address nPDFs (see a detailed comparison in Sect. IV).

The present work extends the calculation of nPDFs of [9] with an emphasis on the theoretical ambiguity and accuracy of the predictions and makes a comparison to fixed-target nuclear DIS data. In particular, we demonstrate that

- The theory of leading twist nuclear shadowing and QCD analysis of hard diffraction at HERA enable one to predict in a model-independent way the next-to-leading order nPDFs for $10^{-5} \leq x \lesssim 10^{-2}$ with 30% accuracy, Fig. 6. For larger x , $10^{-2} \leq x \leq 0.1 - 0.2$, there appears an additional effect of nuclear antishadowing that requires modeling and whose uncertainty is larger. In addition, the HERA diffractive data for $x_P > 0.01$ contains a sub-leading Reggeon contribution, which adds additional ambiguity to our predictions, especially for $x > 0.01$.
- The interactions with $N \geq 3$ nucleons (which is a model-dependent element of the Gribov approach) give negligible contribution in the NMC fixed-target nuclear DIS kinematics, see Fig. 8. The A -dependence of the NMC data for $x \sim 0.01$ is reasonably well reproduced, see Fig. 13.
- The failure to describe the absolute value of the $F_2^A/(AF_2^N)$ ratios of the available fixed-target data for $0.003 < x < 0.02$ and $Q^2 < 3 \text{ GeV}^2$ likely indicates the presence of significant higher twist effects in the data. Indeed, when the leading twist shadowing is complemented by higher twist effects, which are modeled by ρ , ϕ and ω meson contributions in the spirit of vector meson dominance, the agreement with the data becomes fairly good, see Figs. 10, 11 and 12. All this signals that any leading twist QCD analysis of the available data is unreliable for $0.003 < x < 0.02$.
- The next-to-leading order (NLO) effects in the $F_2^A/(AF_2^N)$ ratios are found to be quite sizable. This means that it is not self-consistent to use the leading order parameteri-

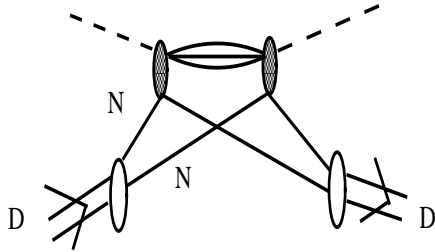


FIG. 1: Gribov's theorem [6]: The forward hadron-deuteron rescattering amplitude, which gives rise to nuclear shadowing, is proportional to the differential hadron-nucleon diffractive cross section at $t \sim 0$.

zations of nPDFs in the NLO QCD calculations, see Fig. 15.

In short, the main goals of the paper are to give a concise summary of the leading twist theory of nuclear shadowing, to assess the theoretical uncertainties of the resulting predictions and to make a comparison to nuclear DIS data. We attempted to give a self-contained presentation and, hence, this paper can be rightfully considered as a *guide* to leading twist nuclear shadowing.

II. LEADING TWIST THEORY OF NUCLEAR SHADOWING

In this section, we review the leading twist approach to nuclear shadowing developed in [8] and further elaborated on in [9].

The approach is based on the 1969 work by V. Gribov [6], where the following theorem was proven. Let us consider hadron-deuteron scattering at high energies within the approximation that the radius of the deuteron is much larger than the range of the strong interaction. Then the shadowing correction to the total cross section is expressed in terms

of the differential diffractive hadron-nucleon cross section. This is demonstrated in Fig. 1: The forward hadron-deuteron rescattering amplitude giving rise to the nuclear shadowing correction contains the hadron-nucleon diffractive amplitude (denoted by the shaded blob) squared.

The relationship between nuclear shadowing and diffraction was used in the analysis of parton densities of deuterium and other nuclei by Frankfurt and Strikman in [8]. For deuterium and other sufficiently light (low nuclear density) nuclei, nuclear shadowing and diffraction on the nucleon are related in a model-independent way using the Gribov theorem [57].

The generalization to heavy nuclei involves certain modeling of multiple rescattering contributions, which, however, is under control [23]. Below we shall recapitulate the derivation of the leading twist nuclear shadowing for nPDFs, which can be carried out in three steps.

Step 1. The shadowing correction arising from the coherent interaction with any two nucleons of the nuclear target with the atomic mass number A , $\delta F_{2A}^{(2)}$ (the superscript (2) serves as a reminder that only the interaction with two nucleons is accounted for), is expressed in terms of the proton diffractive structure function $F_2^{D(4)}$ (the superscript (4) indicates the dependence on four kinematic variables) as a result of the generalization of the Gribov result for deuterium (see also Ref. [10]). This does not require decomposition over twists and is therefore valid even for the case of real photon interactions. The shadowing correction $\delta F_{2A}^{(2)}$ reads [58]

$$\delta F_{2A}^{(2)}(x, Q^2) = \frac{A(A-1)}{2} 16\pi \mathcal{R} e \left[\frac{(1-i\eta)^2}{1+\eta^2} \int d^2b \int_{-\infty}^{\infty} dz_1 \int_{z_1}^{\infty} dz_2 \int_x^{x_{\mathcal{P},0}} dx_{\mathcal{P}} \right. \\ \left. \times F_2^{D(4)}(\beta, Q^2, x_{\mathcal{P}}, t)|_{t=t_{\min}} \rho_A(b, z_1) \rho_A(b, z_2) e^{ix_{\mathcal{P}} m_N (z_1 - z_2)} \right], \quad (1)$$

with η the ratio of the real to imaginary parts of the diffractive scattering amplitude; z_1 , z_2 and \vec{b} the longitudinal (in the direction of the incoming virtual photon) and transverse coordinates of the nucleons involved (defined with respect to the nuclear center); β , $x_{\mathcal{P}}$ and t the usual kinematic variables used in diffraction. Throughout this work, we use $\beta = x/x_{\mathcal{P}}$. Equation (1) uses the fact that the t -dependence of the elementary diffractive amplitude is much weaker than that of the nuclear wave function, and, hence, $F_2^{D(4)}$ can be approximately evaluated at $t = t_{\min} \approx 0$. All information about the nucleus is encoded in the nucleon distributions $\rho_A(b, z_i)$, see Appendix A for details. Finally, $x_{\mathcal{P},0}$ is a cut-off

parameter ($x_{P,0} = 0.1$ for quarks and $x_{P,0} = 0.03$ for gluons), which will be discussed later in the text.

The origin of all factors in Eq. (1) can be readily seen by considering the corresponding forward double rescattering Feynman diagram (see Fig. 2), which accounts for the diffractive production of intermediate hadronic states by the incoming virtual photon:

- The combinatoric factor $A(A - 1)/2$ is the number of the pairs of nucleons involved in the rescattering process.
- The factor 16π provides the correct translation of the differential diffractive to the total rescattering cross section (see the definition later), as required by the Glauber theory [10, 24].
- The factor $(1 - i\eta)^2/(1 + \eta^2)$ is a correction for the real part of the diffractive scattering amplitude \mathcal{A} . Since the shadowing correction is proportional to $(Im\mathcal{A})^2$, while the total diffractive cross section is proportional to $|\mathcal{A}|^2$, the factor $(1 - i\eta)^2/(1 + \eta^2)$ emerges naturally, when one expresses nuclear shadowing in terms of the total diffractive cross section (diffractive structure function).
- The integration over the positions of the nucleons is the same as in the Glauber theory. Similarly, because the recoil of the nucleons is neglected (the transverse radius of the elementary strong amplitude is much smaller than the scale of the variation of the nuclear density), both involved nucleons have the same transverse coordinate \vec{b} .
- The integration over x_P represents the sum over the masses of the diffractively produced intermediate states.
- In order to contribute to nuclear shadowing (not to break up the nucleus in its transition from the |in>-state to the <out|-state), the virtual photon should interact with the nucleons diffractively. The product of the two diffractive amplitudes (depicted as shaded blobs in Fig. 2) gives the diffractive structure function of the proton $F_2^{D(4)}$. Also note that we do not distinguish between diffraction on the proton and neutron in the present work, as the corresponding diffractive amplitudes are equal at small x .
- The effect of the nucleus is given by the nucleon densities $\rho_A(b, z_i)$. For the sufficiently heavy nuclei that we consider, nucleon-nucleon correlations can be neglected and the

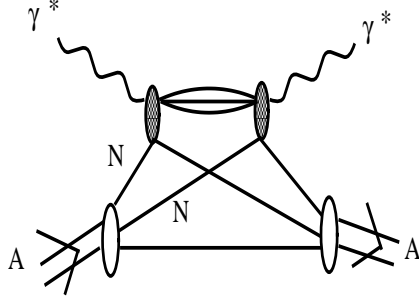


FIG. 2: The forward γ^* -nucleus rescattering amplitude that gives the principal contribution to nuclear shadowing.

nuclear wave function squared can be approximated well by the product of individual $\rho_A(b, z_i)$ for each nucleon (the so-called independent particle approximation).

- The factor $e^{ix_P m_N(z_1 - z_2)}$ is a consequence of the propagation of the diffractively produced intermediate state between the two nucleons involved.

Step 2. The QCD factorization theorems for inclusive [25] and hard diffractive DIS [7] can be used to relate the structure functions in Eq. (1) to the corresponding – inclusive and diffractive – parton distribution functions. Since the coefficient functions (hard scattering parts) are the same for both inclusive and diffractive structure functions, the relation between the shadowing correction to nPDFs and the proton diffractive parton distribution functions (PDFs) is given by an equation similar to Eq. (1). The shadowing correction to the nPDF of flavor j , $f_{j/A}$, $\delta f_{j/A}^{(2)}$, is related to the proton (nucleon) diffractive PDF $f_{j/N}^{D(4)}$ of the same flavor

$$\delta f_{j/A}^{(2)}(x, Q^2) = \frac{A(A-1)}{2} 16\pi \mathcal{R}e \left[\frac{(1-i\eta)^2}{1+\eta^2} \int d^2b \int_{-\infty}^{\infty} dz_1 \int_{z_1}^{\infty} dz_2 \int_x^{x_{P,0}} dx_P \right. \\ \left. \times f_{j/N}^{D(4)}(\beta, Q^2, x_P, t)|_{t=t_{\min}} \rho_A(b, z_1) \rho_A(b, z_2) e^{ix_P m_N(z_1 - z_2)} \right]. \quad (2)$$

Equation (2) is very essential in several ways. Firstly, it enables one to evaluate nuclear shadowing for each parton flavor j separately. Secondly, since the diffractive PDFs obey leading twist QCD evolution, so does the shadowing correction $\delta f_{j/A}^{(2)}$. This explains why the considered theory can be legitimately called the leading twist approach. Since Eq. (2) is based on the QCD factorization theorem, it is valid to all orders in α_s . Hence, if $f_{j/N}^{D(4)}$ is known with the next-to-leading order (NLO) accuracy, as is the case for the used H1 parameterization for $f_{j/N}^{D(4)}$, we can readily make predictions for NLO nPDFs.

Step 3. Equation (2) is derived in the approximation of the low nuclear thickness, and it takes into account only the interaction with two nucleons of the target. The effect of the rescattering on three and more nucleons can be taken into account by introducing the attenuation factor $T(b, z_1, z_2)$ (see for example [10]),

$$T(b, z_1, z_2) = e^{-(A/2)(1-i\eta)\sigma_{\text{eff}}^j \int_{z_1}^{z_2} dz \rho_A(b, z)}, \quad (3)$$

where the meaning of σ_{eff}^j should become clear after the following discussion. Let us consider sufficiently small values of Bjorken variable x such that the factor $e^{ix_{\mathbb{P}}m_N(z_1-z_2)}$ in Eq. (2) can be neglected. Then, introducing σ_{eff}^j as

$$\sigma_{\text{eff}}^j(x, Q^2) = \frac{16\pi}{f_{j/N}(x, Q^2)(1 + \eta^2)} \int_x^{x_{\mathbb{P},0}} dx_{\mathbb{P}} f_{j/N}^{D(4)}(\beta, Q^2, x_{\mathbb{P}}, t)|_{t=t_{\text{min}}}, \quad (4)$$

Eq. (2) can be written in the form equivalent to the usual Glauber approximation

$$\begin{aligned} \delta f_{j/A}^{(2)}(x, Q^2) &\approx \frac{A(A-1)}{2} (1 - \eta^2) \sigma_{\text{eff}}^j(x, Q^2) f_{j/N}(x, Q^2) \\ &\times \int d^2b \int_{-\infty}^{\infty} dz_1 \int_{z_1}^{\infty} dz_2 \rho_A(b, z_1) \rho_A(b, z_2), \end{aligned} \quad (5)$$

where $f_{j/N}$ is the proton inclusive PDF. Therefore, it is clear that thus introduced σ_{eff}^j has the meaning of the rescattering cross section, which determines the amount of nuclear shadowing in the approximation of Eq. (5). Hence, it is natural to assume that the same cross section describes rescattering with the interaction with three and more nucleons, as postulated by the definition of the attenuation factor $T(b, z_1, z_2)$ by Eq. (3). In the language of Feynman diagrams, the assumed form of the attenuation factor implies that the diffractively produced intermediate state rescatters without a significant change of mass with the same cross section on all remaining nucleons of the target, as depicted in Fig. 3 for the case of the triple scattering. The approximation of elastic rescattering is not important at small enough x where longitudinal distances are much larger than the nuclear size, see discussion below.

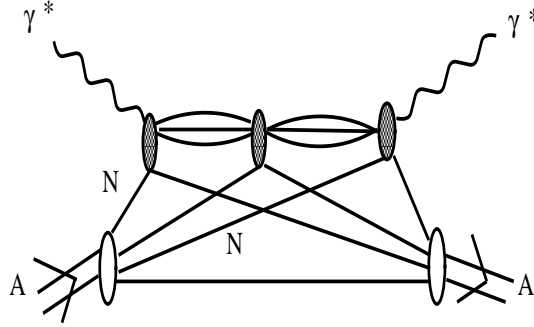


FIG. 3: The forward γ^* -nucleus triple scattering amplitude.

Corrections to the elastic rescattering approximation can be estimated by taking into account the effects of fluctuations of the strength of the rescattering interaction. Modeling of these effects was performed in [23] with the conclusion that for a wide range of cross section fluctuations, the reduction of nuclear shadowing (for fixed σ_{eff}) remains a rather small correction for all nuclei.

After introducing the attenuation factor into Eq. (2), the complete expression for the shadowing correction, $\delta f_{j/A}$, becomes

$$\delta f_{j/A}(x, Q^2) = \frac{A(A-1)}{2} 16\pi \mathcal{R} e \left[\frac{(1-i\eta)^2}{1+\eta^2} \int d^2b \int_{-\infty}^{\infty} dz_1 \int_{z_1}^{\infty} dz_2 \int_x^{x_{P,0}} dx_{\mathcal{P}} \right. \\ \left. \times f_{j/N}^{D(4)}(\beta, Q^2, x_{\mathcal{P}}, t_{\min}) \rho_A(b, z_1) \rho_A(b, z_2) e^{ix_{\mathcal{P}} m_N (z_1 - z_2)} e^{-(A/2)(1-i\eta) \sigma_{\text{eff}}^j \int_{z_1}^{z_2} dz \rho_A(b, z)} \right]. \quad (6)$$

This is our master equation (see also Eq. (14)). It contains several sources of model-dependence and theoretical ambiguity. First, the attenuation factor $T(b, z_1, z_2)$ assumes that multiple rescatterings can be described by a single rescattering cross section [59] σ_{eff}^j , i.e. cross section fluctuations are neglected in the interaction with three and more nucleons. Note that in the phenomenologically important kinematic region of fixed-target experiments, $x > 0.01$ and $Q^2 > 2 \text{ GeV}^2$, the uncertainty associated with the attenuation factor $T(b, z_1, z_2)$ is negligible since the rescattering contribution to shadowing is small, see Fig. 8. Second, the

necessity to introduce the parameter $x_{P,0}$ is a consequence of the fact that Eq. (6) applies only to the region of nuclear shadowing: The transition to the region of the enhancement of nPDFs should be modeled separately. This is the role of the parameter $x_{P,0}$. Third, there are experimental uncertainties in the determination of the diffractive PDFs $f_{j/N}^{D(4)}$ which we use as an input in Eq. (6).

Equation (6) defines the input nPDFs for the DGLAP evolution equations. As a starting evolution scale Q_0^2 , we take $Q_0^2 = 4 \text{ GeV}^2$: This is the lowest value of Q^2 of the H1 diffractive fit [29]. Nuclear PDFs at $Q^2 > Q_0^2$ are obtained using the NLO QCD evolution equations. Therefore, we predict that nuclear shadowing is a leading twist phenomenon.

In the small- x limit, which for practical purposes means $x < 10^{-3}$, the factor $e^{ix_{P,m_N}(z_1-z_2)}$ in Eq. (6) can be safely omitted, which results in a significant simplification of the master formula (after integration by parts two times)

$$\delta f_{j/A}(x, Q^2) = \frac{2(1-1/A) f_{j/N}(x, Q^2)}{\sigma_{\text{eff}}^j} \text{Re} \left(\int d^2b (e^{-LT(b)} - 1 + LT(b)) \right), \quad (7)$$

where $L = A/2(1-i\eta)\sigma_{\text{eff}}^j$; $T(b) = \int_{-\infty}^{\infty} dz \rho_A(b, z)$.

In the heavy nucleus limit ($A \rightarrow \infty$) and at fixed σ_{eff} ,

$$\frac{f_{j/A}(x, Q^2)}{A f_{j/N}(x, Q^2)} = 1 - \frac{\delta f_{j/A}(x, Q^2)}{A f_{j/N}(x, Q^2)} = \frac{2\pi R_A^2}{A \sigma_{\text{eff}}^j}, \quad (8)$$

where R_A is the nuclear size. As can be seen, in the theoretical limit of infinitely heavy nucleus, nuclear shadowing equals the ratios of the nuclear to nucleon sizes, i.e. it is a purely geometrical effect. At the same time, in the $Q^2 = \text{const}$, $W \rightarrow \infty$ limit, when the leading twist approximation is violated and the radius of the strong interaction becomes larger than R_A , the $\sigma_{\gamma^*A}/\sigma_{\gamma^*N}$ ratio should approach unity [26].

III. PARAMETERS AND UNCERTAINTIES OF THE METHOD

The master equation (6) uses as input the information on hard diffraction in DIS on the proton, which was measured at HERA by ZEUS [27] and H1 [28] collaborations. We use the H1 parameterization of $f_{j/N}^{D(3)}$ [29] (note the superscript (3) indicating that the t -dependence of diffraction is not measured), which is based on the QCD analysis of the 1994 H1 data [28] (we use Fit B, see Appendix A of Ref. [9]). The choice of the H1 parameterization is motivated by the following observations:

- It is available in an easily accessible and usable form, see [29] and also Appendix A of Ref. [9].
- The diffractive jet production in DIS at HERA data [30] is best described by the H1 parameterization. The fit of Alvero, Collins, Terron and Whitmore [31] somewhat overestimates the data. Another parameterization available in the literature, that of Hautmann, Kunszt and Soper [32], is not based on the detailed fit to the available diffractive data.
- The 1994 H1 fit is in a fair agreement with the most recent 1997 H1 data [33]. However, the 1997 H1 data indicates that the gluon distribution of the 1994 fit is too large by about 25%. Hence, in our analysis we multiplied the gluon diffractive distribution of [29] by 0.75.

Since the diffractive PDF $f_{j/N}^{D(4)}$ enters Eq. (6) at $t \approx 0$, one has to assume a certain t -dependence in order to be able to use the H1 results for the t -integrated $f_{j/N}^{D(3)}$. The common choice is to assume that

$$f_{j/N}^{D(4)}(\beta, Q^2, x_{\mathcal{P}}, t) = e^{B_j t} f_{j/N}^{D(4)}(\beta, Q^2, x_{\mathcal{P}}, t \approx 0), \quad (9)$$

so that after the integration over t , one obtains

$$f_{j/N}^{D(4)}(\beta, Q^2, x_{\mathcal{P}}, t \approx 0) = B_j f_{j/N}^{D(3)}(\beta, Q^2, x_{\mathcal{P}}), \quad (10)$$

where B_j is the slope of the t -dependence of $f_{j/N}^{D(4)}$. A priori there is no reason why the slope B_j should be equal for all parton flavors j and, hence, we introduce its explicit flavor dependence. In our analysis we use the following values for B_j . For all quark flavors, we use $B_q = 7.2 \pm 1.1(\text{stat.})_{-0.9}^{+0.7}(\text{syst.}) \text{ GeV}^{-2}$, which is determined by the measurement of the t -dependence of the diffractive structure function $F_2^{D(4)}$, as measured by the ZEUS collaboration [34]. Of course, the diffractive slope should increase with decreasing x (diffractive cone shrinkage). However, since the experimental error of the value of B_q is large and no measurements of the x -dependence of B_q are available, any theoretically expected logarithmic increase of B_q will be within the quoted experimental errors. Hence, it is sufficient to use the x -independent B_q .

The slope of the gluon PDF, B_g , could be different from B_q . If the gluon-induced diffraction is dominated by small-size (compared to typical soft physics sizes) partonic configurations in the projectile, B_g could as low as the slope of J/ψ diffractive production measured

at HERA which is substantially lower than B_q . To reflect the uncertainties in the value of B_g we examined two scenarios: $B_g = 4 + 0.2 \ln(10^{-3}/x) \text{ GeV}^{-2}$ and $B_g = 6 + 0.25 \ln(10^{-3}/x) \text{ GeV}^{-2}$. The first one corresponds to the lower end of the values of the J/ψ photoproduction slope reported at HERA [35], while the second one is close to B_q and to the J/ψ slope reported in [36].

The analysis of recent ZEUS data on the slope of $F_2^{D(4)}$ [37] reports the values similar to those reported in [34]. The analysis also provides information on the x_P -dependence of the slope though not on the β -dependence of the slope (average β for the data sample is growing with a decrease of x_P). Overall, the data appear to be consistent with the Regge factorization and for the most of the x_P range, the gluon diffractive PDF appears to give a significant, if not the dominant, contribution. This suggests that our model with a higher value of B_g is closer to the data, though in view of the lack of the data on the slope of the gluon induced diffraction at large β , we feel necessary to keep the lower B_g model as well.

The analysis of the 1994 H1 data [28] showed that at large x_P , the successful fit to the data requires both the Pomeron and the Reggeon contributions. In our numerical analysis we include only the dominant Pomeron part, because the subleading Reggeon contribution begins to play a role only for $x > 0.01$, where the theoretical ambiguities are large anyway. Therefore, in our analysis we use the Reggeon contribution only to estimate its contribution to the overall uncertainty of our predictions, see Appendix B for details.

Using Eq. (10), the rescattering cross section σ_{eff}^j becomes

$$\sigma_{\text{eff}}^j(x, Q^2) = \frac{16\pi B_j}{f_{j/N}(x, Q^2)(1 + \eta^2)} \int_x^{x_{P,0}} dx_P f_{j/N}^{D(3)}(\beta, Q^2, x_P), \quad (11)$$

where η is the ratio of the real to imaginary parts of the diffractive amplitude \mathcal{A} . This ratio can be related to the intercept of the effective Pomeron trajectory, $\alpha_P(0)$, using the Gribov-Migdal result [38]

$$\eta \approx \frac{\pi}{2}(\alpha_P(0) - 1) = 0.32, \quad (12)$$

where the H1 value for $\alpha_P(0)$ was employed.

The results of the evaluation of σ_{eff}^j are presented in Fig. 4. The left panel presents σ_{eff} for anti u -quarks and the right panel is for the gluons, both cases for $Q^2 = 4 \text{ GeV}^2$. The error bands around the central curves represent the uncertainty in the determination of σ_{eff} . This uncertainty comes from the uncertainties in B_q , $f_{j/N}^{D(3)}(\beta, Q^2, x_P)$ (taken to be 25%)

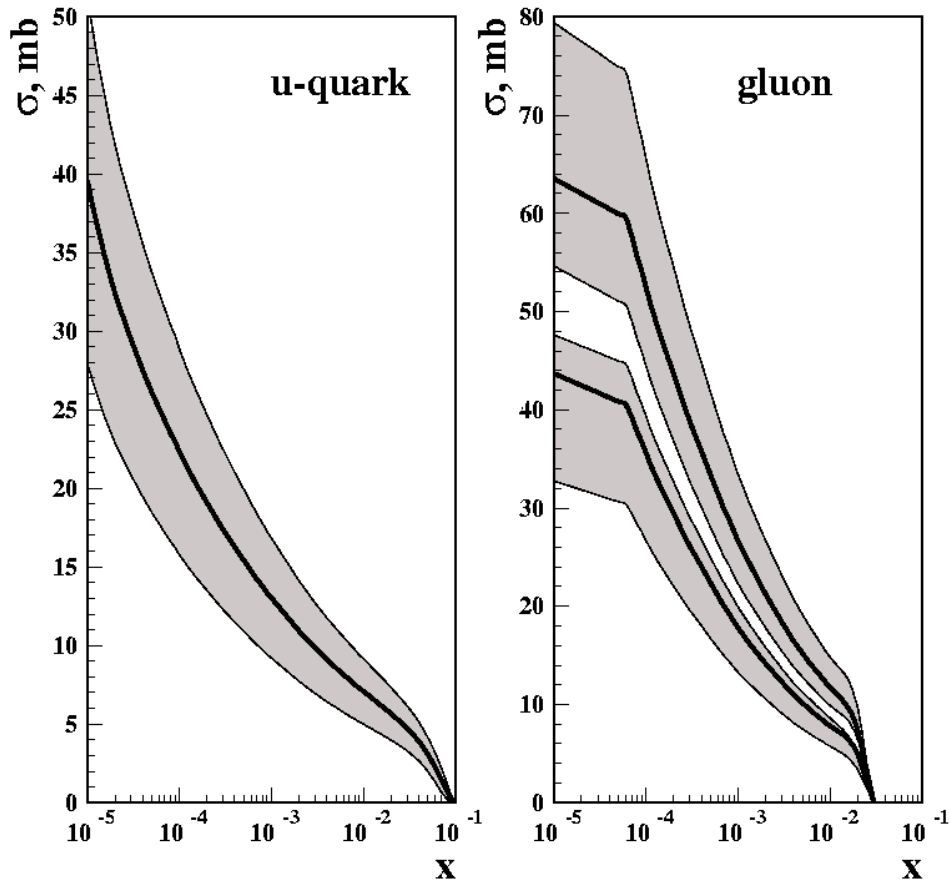


FIG. 4: The effective cross section σ_{eff} for the anti u -quark and gluon channels at $Q_0^2 = 4 \text{ GeV}^2$. The error bands represent the uncertainty in the predictions discussed in the text.

and the choice of $x_{P,0}$ added in quadrature. Two solid curves for the gluon case correspond to the two scenarios for the slope B_g discussed above.

Now we would like to examine which values of the diffractive masses or β contribute to σ_{eff} . At very high energies (small x), one enters the regime analogous to the triple Pomeron limit of hadronic physics, which corresponds to $\beta = Q^2/(Q^2 + M_X^2) \ll 1$. In this case, one may need to resum logs of energy in the diffractive block (logs of β). However, deviations from DGLAP are expected only for $\beta \leq 10^{-3}$, which is beyond the x range that we consider [39]. At extremely small x , the contribution of small β may become dominant. This contribution was evaluated within Color Condensate model in [40] neglecting the large β contribution.

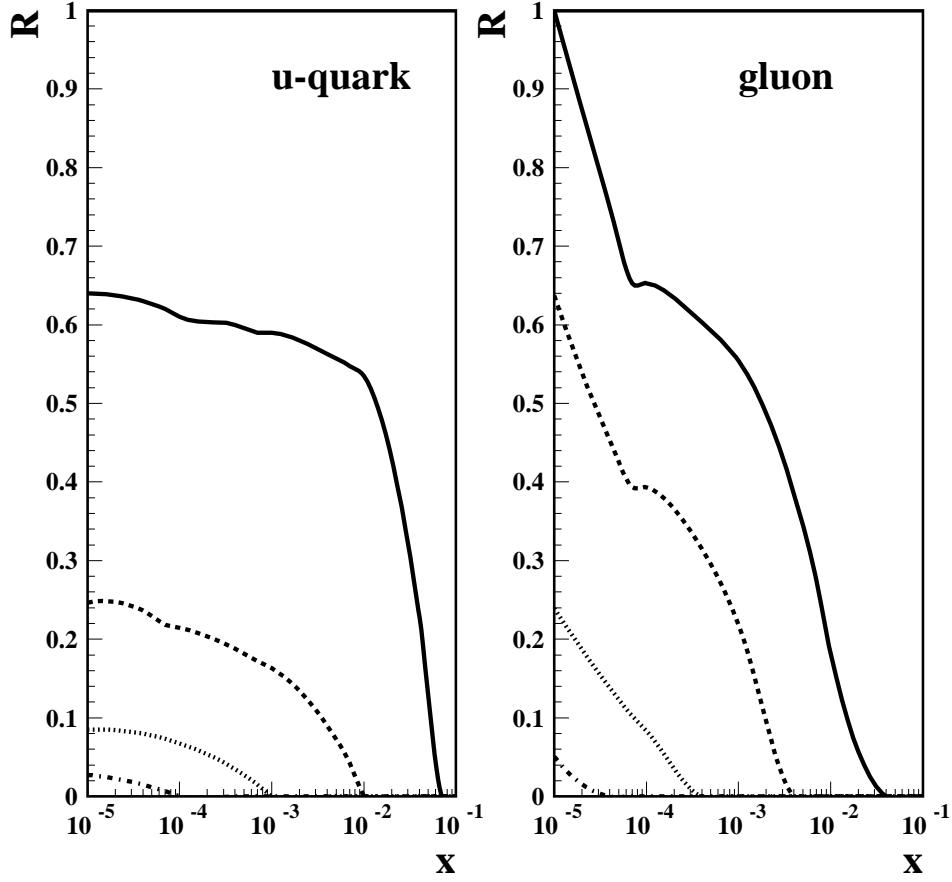


FIG. 5: The ratio R at $Q_0^2 = 4 \text{ GeV}^2$. The solid curves correspond to $\beta_{\max} = 0.5$; the dashed curves correspond to $\beta_{\max} = 0.1$; the dotted curves correspond to $\beta_{\max} = 0.01$; the dot-dashed curves correspond to $\beta_{\max} = 0.001$.

To analyze at what x small β become dominant, it is convenient to introduce the ratio R defined as follows

$$R(\beta_{\max}, x) = \frac{\int_x^{x_{P,0}} dx_{\mathcal{P}} f_{j/N}^{D(3)}(\beta, Q^2, x_{\mathcal{P}}) \Theta(\beta_{\max} - \beta)}{\int_x^{x_{P,0}} dx_{\mathcal{P}} f_{j/N}^{D(3)}(\beta, Q^2, x_{\mathcal{P}})}. \quad (13)$$

The ratio R for u -quark and gluon channels at $Q_0^2 = 4 \text{ GeV}^2$ is presented in Fig. 5. In the figure, the solid curves correspond to $\beta_{\max} = 0.5$; the dashed curves correspond to $\beta_{\max} = 0.1$; the dotted curves correspond to $\beta_{\max} = 0.01$; the dot-dashed curves correspond to $\beta_{\max} = 0.001$.

From Fig. 5 one can see how much different β -regions contribute to nuclear shadowing. For instance, taking $x = 10^{-3}$, which roughly corresponds to the smallest x which could be reached in the RHIC kinematics, one sees that large diffractive masses that correspond to $\beta \leq 0.1$ (dashed curve) contribute 20% to nuclear shadowing in the quark channel and 30% to nuclear shadowing in the gluon channel. Therefore, Fig. 5 indicates that if the Color Glass Condensate model is implemented in a way consistent with the HERA diffractive data, it predicts a very small fraction of total shadowing for the RHIC kinematic range.

For completeness, we rewrite our master equation, Eq. (6), in the form which explicitly includes the diffractive slope B_j

$$\delta f_{j/A}(x, Q^2) = \frac{A(A-1)}{2} 16B_j \pi \mathcal{R} e \left[\frac{(1-i\eta)^2}{1+\eta^2} \int d^2b \int_{-\infty}^{\infty} dz_1 \int_{z_1}^{\infty} dz_2 \int_x^{x_{P,0}} dx_P \right. \\ \left. \times f_{j/N}^{D(3)}(\beta, Q^2, x_P) \rho_A(b, z_1) \rho_A(b, z_2) e^{ix_P m_N (z_1 - z_2)} e^{-(A/2)(1-i\eta)\sigma_{\text{eff}}^j \int_{z_1}^{z_2} dz \rho_A(b, z)} \right]. \quad (14)$$

We would like to point out that while the leading twist theory of nuclear shadowing is applicable to the partons of all flavors, see Eq. (14), using the low- x HERA diffractive data, which is heavily dominated by the Pomeron contribution, we cannot make any quantitative predictions for nuclear shadowing of the valence quarks in nuclei. Nuclear shadowing for the valence quarks is driven by the t -channel exchanges with non-vacuum quantum numbers (Reggeon contribution), whose contribution is largely lost in the kinematic region of the HERA data. In practical terms, this means that Eq. (14) should be applied to evaluate nuclear shadowing for the antiquarks and gluons only.

As mentioned above, Eq. (14) cannot describe nuclear modifications of PDFs at $x > 0.1$ for the quarks and $x > 0.03$ for the gluons, where nuclear antishadowing and the EMC effects dominate. For a comprehensive picture of nuclear modification for all values of x , we refer the reader to the review in [14]. However, since we use Eq. (14) to evaluate nPDFs at some input scale for QCD evolution, in order to provide sensible results after the evolution, we should have a reasonable estimate of nPDFs for all x . We adopted the picture of nuclear modification of PDFs developed in [11, 41], which suggests that antiquarks in nuclei are not enhanced and the gluons are antishadowed and which uses the constraints based on the baryon and energy-momentum conservation sum rules. In our case, like in [9], we model the enhancement of the gluon nPDF in the interval $0.03 \leq x \leq 0.2$ with a simple function $a(0.2-x)(x-0.03)$ and choose the free coefficient a by requiring the conservation of the momentum sum rule for nPDFs. For instance for ^{40}Ca , this requirement gives $a \approx 30$ and

about 2-3% enhancement of the fraction of the total momentum of the nucleus carried by the gluons, in accord with the analysis of [11].

IV. LEADING TWIST NPDFS AND STRUCTURE FUNCTIONS

The master equation (14) allows one to determine NLO nPDFs at the input scale $Q_0^2 = 4$ GeV². As an example of such a calculation, we present ratios of the nuclear (Ca-40) to free proton PDFs and the ratio of the nuclear to the free nucleon structure function, $F_2^N = (F_2^p + F_2^n)/2$, at $Q^2 = 4$ GeV² by solid curves in Fig. 6. The shaded error bands around the solid curves indicate the uncertainty of the predictions. For comparison, LO predictions of Eskola *et al.* [1] (based on the LO fit to the DIS and Drell-Yan nuclear data) for the corresponding ratios are given by the dashed curves.

Note that for the gluon ratio, we give two predictions corresponding to two versions of the diffractive slope B_g discussed earlier. Also, since we do not predict nuclear shadowing for the valence quarks, this information should be taken from elsewhere. In our analysis, we use the parameterization by Eskola *et al.* [1] (see the upper left panel).

For the parameterization of the proton PDFs, we used the NLO fit CTEQ5M [42].

Figure 7 presents the Q^2 -evolution of the ratios in Fig. 6. The solid curves correspond to $Q^2 = 4$ GeV²; the dashed curves correspond to $Q^2 = 10$ GeV²; the dot-dashed curves correspond to $Q^2 = 100$ GeV². The leading twist character of the predicted nuclear shadowing is apparent from this figure: The shadowing correction decreases slowly with increasing Q^2 and there is still rather significant nuclear shadowing at $Q^2 = 100$ GeV².

One can see from Fig. 6 that our predictions at the lowest values of Bjorken x significantly differ from those by Eskola *et al.* However, one should keep in mind that we make our predictions to the NLO accuracy, while the fitting to the nuclear DIS data in [1] is done to the LO accuracy. One should also note that the parameterization of Eskola *et al.* [1] assumes that at small x , the ratios $F_2^A/(AF_2^N)$ and $g_A/(Ag_N)$ become equal and stay constant (saturate). We point out that:

- Figure 6 presents our predictions for the shapes of the nPDFs for ⁴⁰Ca, which are to be used as an input for QCD evolution at the scale $Q_0 = 2$ GeV. This choice of Q_0 is motivated by the fact that the 1994 H1 diffractive data has $Q^2 \geq 4.5$ GeV² and the QCD fit to the data of [29] starts at $Q^2 = 3$ GeV². Results of such evolution are

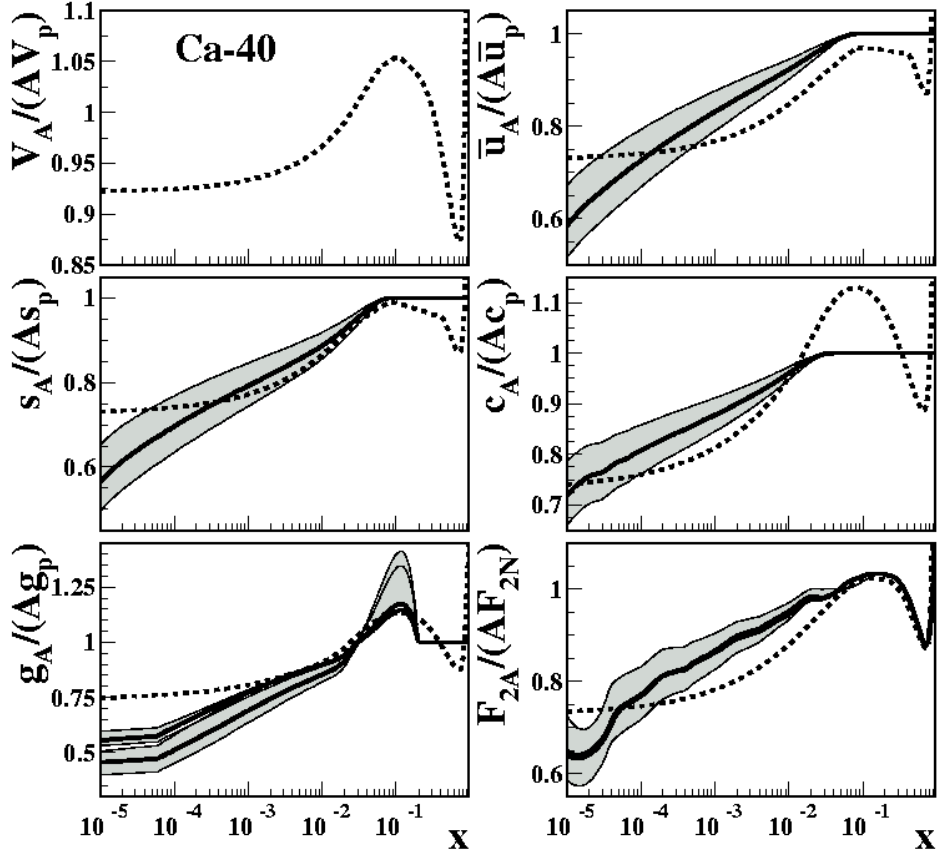


FIG. 6: The ratio of nuclear to proton NLO parton distributions and the nuclear to free nucleon inclusive structure functions F_2 in ^{40}Ca at $Q = 2$ GeV. The leading twist theory results (solid curves and the corresponded shaded error bands) are compared to the LO predictions by Eskola *et al.* [1] (dashed curves).

presented in Fig. 7.

- Leading twist theory predicts much more significant nuclear shadowing for quarks and gluons than the fits to the fixed-target data of Eskola *et al.* [1]. The latter *assumed* that shadowing saturates for small x , e.g. for $x \lesssim 3 \times 10^{-3}$ for ^{40}Ca , and that higher twist effects are negligible.
- Nuclear shadowing for the gluons is larger than for the quarks due to the dominance of gluons in diffractive pdfs (this was further confirmed by the recent ZEUS data [37]).

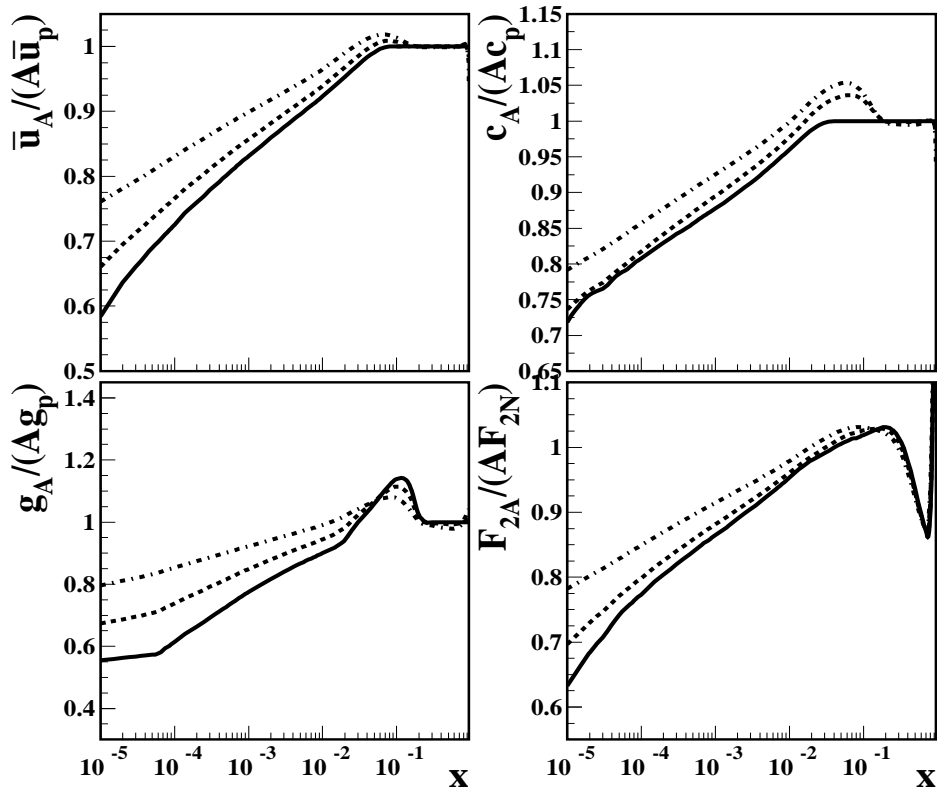


FIG. 7: Scaling violations for nuclear PDFs in ^{40}Ca . The solid curves correspond to $Q^2 = 4 \text{ GeV}^2$; the dashed curves correspond to $Q^2 = 10 \text{ GeV}^2$; the dot-dashed curves correspond to $Q^2 = 100 \text{ GeV}^2$.

- Within our model of antishadowing for the gluons by the simple function $a(0.2-x)(x-0.03)$, significant variations of the parameter a still lead to the conservation (with accuracy better than 1%) of the parton momentum sum rule. Hence, the amount of antishadowing for the gluons is not sensitive to the low- x behavior of the gluons.
- Should we compare our predictions to those by Hirai, Kumano and Miyama or to the updated fit by Hirai, Kumano and Nagai [2], the disagreement in the shadowing predictions, especially for the gluons, would be much larger. For the comparison of the parameterizations of [1] and the first of [2], one can consult [4].
- Comparing to the parameterization suggested in the work of Li and Wang [3], we again find a strong disagreement in the quark channel and, a surprisingly good agreement

for the gluons. However, the parameterization of [3] are not based on the detailed comparison to all available fixed-target data, but rather on the need to fit the RHIC data within the HIJING model. Note also that this parameterization does not include the enhancement either in the quark or gluon channels and, hence, violates the exact QCD momentum sum rule for the parton densities.

- The only NLO QCD fit to nuclear DIS data by de Florian and Sassot [5] produces very small nuclear shadowing for nPDFs, which is inconsistent with our predictions as well as with the predictions of [1, 2, 3].
- Our predictions for nPDFs and the structure function F_2^A for the nuclei of ^{12}C , ^{40}Ca , ^{110}Pd , ^{197}Au and ^{206}Pb and for the kinematic range $10^{-5} \leq x \leq 1$ and $4 \leq Q^2 \leq 10,000$ GeV^2 have been tabulated. They are available in the form of a simple Fortran program from V. Guzey upon request, vadim.guzey@tp2.rub.de, or from V. Guzey's web page, <http://www.tp2.rub.de/~vading/index.html>.

We also study the importance of the effect of multiple rescatterings, which is described by the attenuation factor $T(b)$ in Eq. (14). Figure 8 compares the result of the full calculation of the $\bar{u}_A/(A\bar{u}_N)$ ratio for ^{40}Ca at $Q = 2$ GeV (solid curve) with the calculation, when the rescattering effect was ignored (dashed curve), i.e. $T(b)$ was set to one in Eq. (14). As seen from Fig. 8, the rescattering effect becomes unimportant for $x > 0.005$, i.e. in the kinematics of the fixed-target nuclear DIS experiments.

Nuclear shadowing corrections to nPDFs become significantly larger, when one considers the interactions with the target nucleus at small impact parameters. Indeed, since the density of nucleons in the center of the nucleus is larger than the average nucleon density, choosing small impact parameters corresponds to the increase of the number of scattering centers. Introducing the impact parameter dependent nPDFs, $f_{j/A}(x, Q^2, b)$, as was done in [9]

$$\int d^2b f_{j/A}(x, Q^2, b) = f_{j/A}(x, Q^2), \quad (15)$$

the nuclear shadowing correction to the impact parameter dependent nPDFs can be readily found from Eq. (14) by simply removing the integration over the impact parameter b

$$\delta f_{j/A}(x, Q^2, b) = \frac{A(A-1)}{2} 16B_j \pi \mathcal{R}e \left[\frac{(1-i\eta)^2}{1+\eta^2} \int_{-\infty}^{\infty} dz_1 \int_{z_1}^{\infty} dz_2 \int_x^{x_{P,0}} dx_P \right]$$

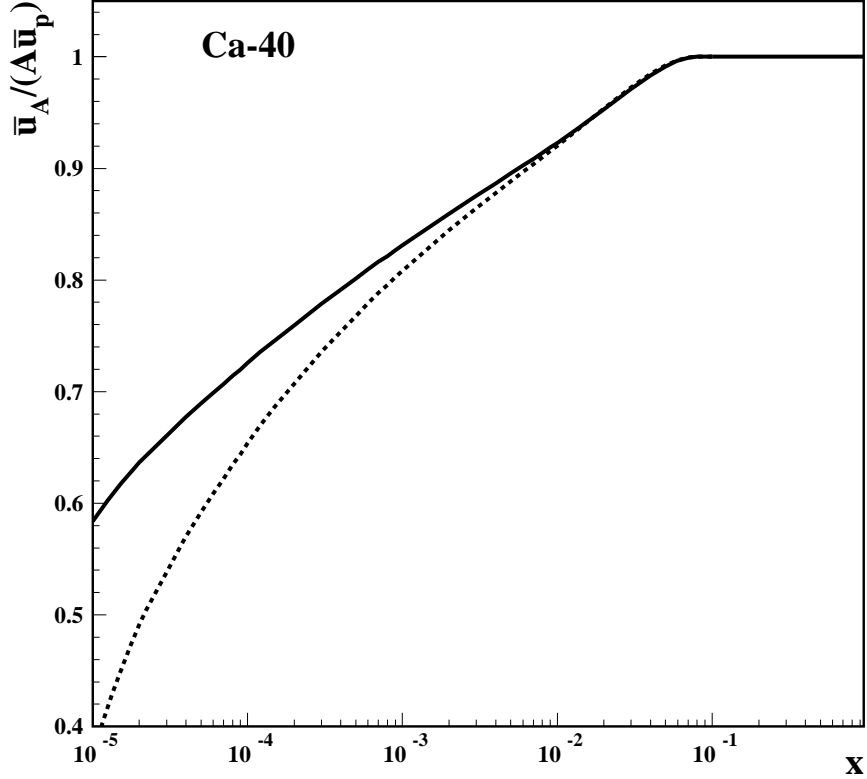


FIG. 8: The $\bar{u}_A/(A\bar{u}_N)$ ratio for ^{40}Ca at $Q = 2$ GeV. The solid curve is the result of the full calculation; the dashed curve is obtained by neglecting multiple rescatterings.

$$\times f_{j/N}^{D(3)}(\beta, Q^2, x_{\mathbf{P}}) \rho_A(b, z_1) \rho_A(b, z_2) e^{ix_{\mathbf{P}} m_N (z_1 - z_2)} e^{-(A/2)(1-i\eta)\sigma_{\text{eff}}^j \int_{z_1}^{z_2} dz \rho_A(b, z)} \Big]. \quad (16)$$

The results of the evaluation of the nuclear shadowing correction using Eq. (16) at the zero impact parameter for anti u -quarks and gluons in ^{197}Au are presented in Fig. 9 in terms of the ratios $\bar{u}_A(x, Q^2, 0)/(AT(0)\bar{u}_N(x, Q^2, 0))$ and $g_A(x, Q^2, 0)/(AT(0)g_N(x, Q^2, 0))$. The solid curves correspond to $Q^2 = 4$ GeV²; the dashed curves correspond to $Q^2 = 10$ GeV²; the dot-dashed curves correspond to $Q^2 = 100$ GeV². Note that the factor $T(0) = \int dz \rho_A(b = 0, z)$ provides the correct normalization of the impulse approximation term, see [9] for details. The impact parameter-dependent nPDFs have been tabulated and are available upon request from V. Guzey or from the following web cite, <http://www.tp2.rub.de/~vading/index.html>. They were already used by R. Vogt in the analysis of the J/ψ production at RHIC and were found to be in a reasonable agreement with the data [43].

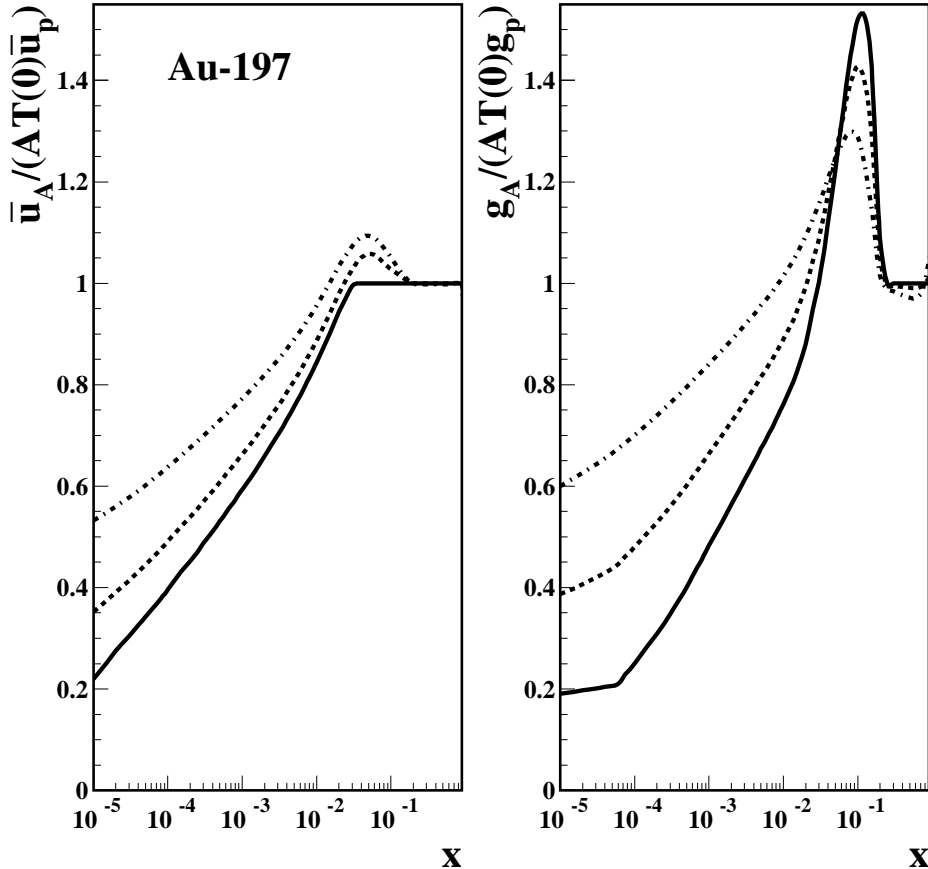


FIG. 9: Nuclear shadowing at zero impact parameter: The ratios $\bar{u}_A(x, Q^2, 0)/(AT(0)\bar{u}_N(x, Q^2, 0))$ and $g_A(x, Q^2, 0)/(AT(0)g_N(x, Q^2, 0))$ for ^{197}Au at $Q^2 = 4 \text{ GeV}^2$ (solid), $Q^2 = 10 \text{ GeV}^2$ (dashed) and $Q^2 = 100 \text{ GeV}^2$ (dot-dashed).

V. COMPARISON TO THE DATA AND EVIDENCE FOR HIGHER TWIST EFFECTS

Our predictions for the $F_2^A/(AF_2^N)$ ratio, where $F_2^N = (F_2^p + F_2^n)/2$, can be compared to the NMC data [44, 45]. However, since the low- x data points correspond to low Q^2 , we cannot make a direct comparison with those points. Therefore, we simply evaluate $F_2^A/(AF_2^N)$ at $Q^2 = Q_0^2 = 4 \text{ GeV}^2$ for the data points with $Q^2 < 4 \text{ GeV}^2$. Figures 10 and 11 compare predictions of our leading twist model (upper set of solid curves with the associated error bands denoted by dashed curves) to the NMC data on ^{12}C and ^{40}Ca [44]; Fig. 12 makes

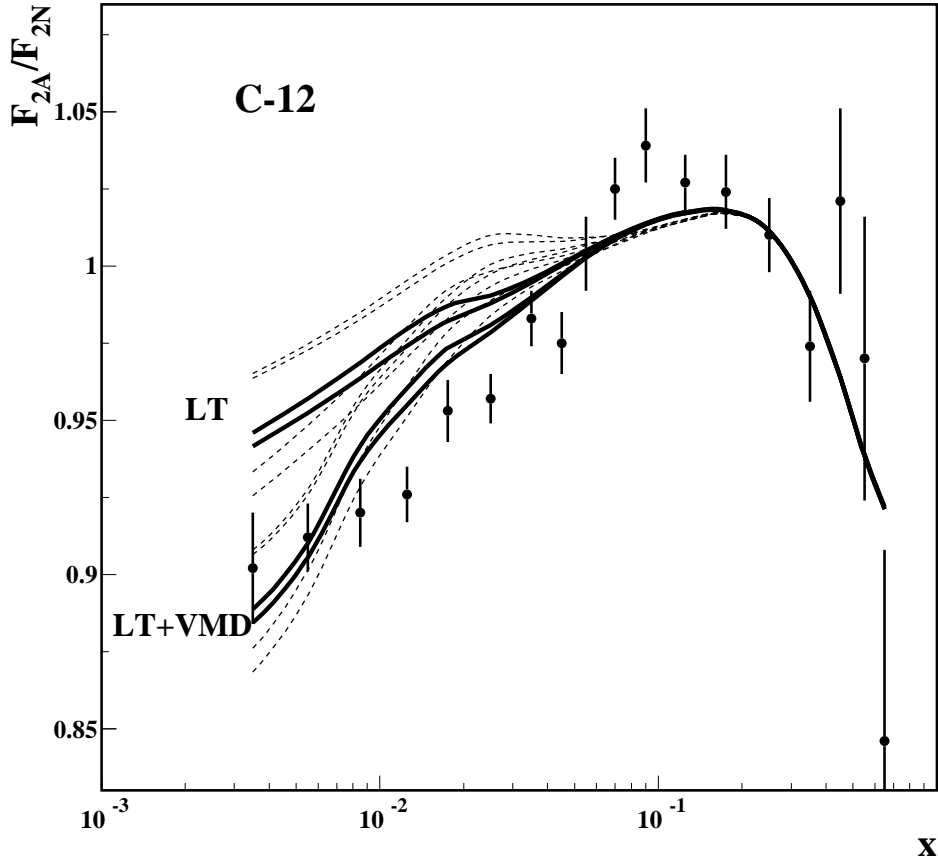


FIG. 10: Comparison of the leading twist theory results (upper set of solid curves and associated dashed error bands) to the NMC data on F_2^{Ca}/F_2^N [44]. The lower set of the solid curves is obtained by adding the VMD contribution using Eq. (18).

a comparison to the NMC $F_2^{Pb}/(F_2^C)$ ratio [45].

One can see from Figs. 10, 11 and 12 that the agreement between the data points and our calculations at low x is poor. Regardless the fact that our model predicts a significant nuclear shadowing effect for low- x , $x < 10^{-3}$, see Fig. 6, nuclear shadowing rather rapidly decreases when x approaches the values of x probed in fixed-target nuclear DIS experiments. Of course, one might argue that we are comparing our predictions at $Q^2 = 4 \text{ GeV}^2$ to the data with much lower Q^2 values. For instance, in Fig. 11 for the first five data points, the average values of Q^2 are $\langle Q^2 \rangle = (0.60, 0.94, 1.4, 1.9, 2.5) \text{ GeV}^2$. We have explicitly checked that the backward QCD evolution of our predictions down to $Q^2 = 2 \text{ GeV}^2$ changes the pre-

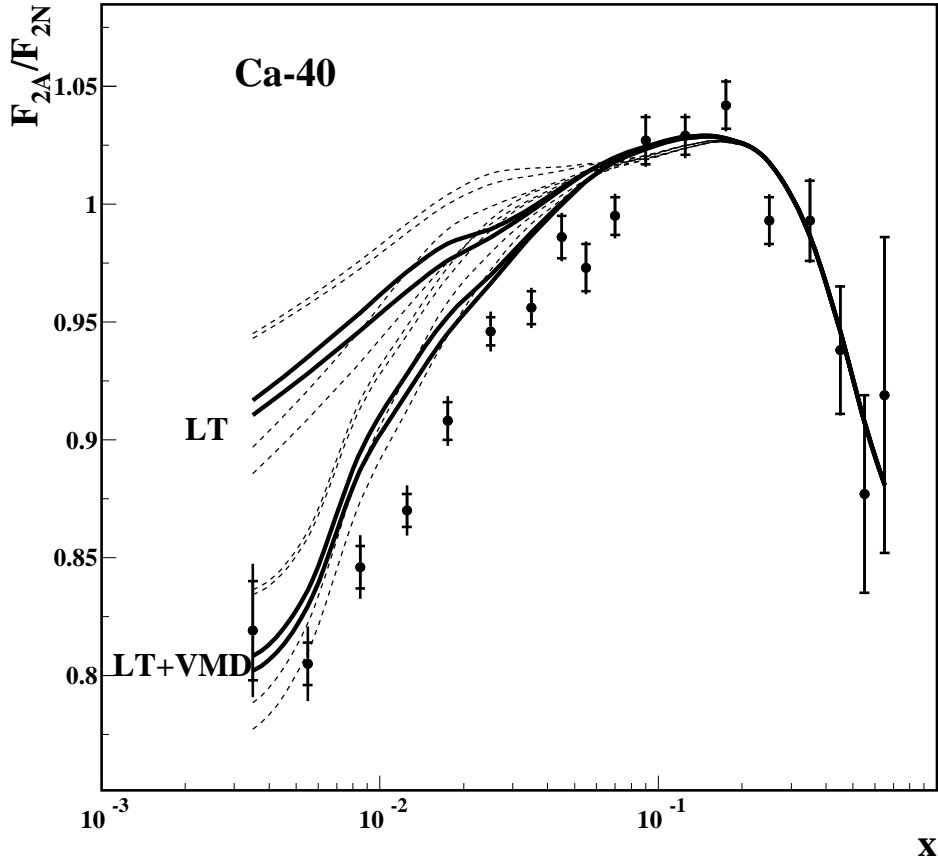


FIG. 11: Comparison of the leading twist theory results (upper set of solid curves and associated dashed error bands) to the NMC data on F_2^{Ca}/F_2^N [44]. The lower set of the solid curves is obtained by adding the VMD contribution using Eq. (18).

dictions only a little. Therefore, since our approach to nuclear shadowing includes the entire leading twist contribution to the nuclear shadowing correction (one should keep in mind a significant uncertainty due to the unaccounted Reggeon contribution, see Appendix B), the disagreement with the NMC low- x data compels us to conclude that *the low- x NMC data [44, 45] could contain significant higher twist effects, which contribute approximately 50% to the nuclear shadowing correction to F_2^A .*

At the same time, the A -dependence is reproduced reasonably well (see below) indicating that the inadequate modeling of the diffraction at low Q^2 and x is to blame. Indeed, it is very natural to have rather significant higher twist effects at small Q^2 since, for this kinematics,

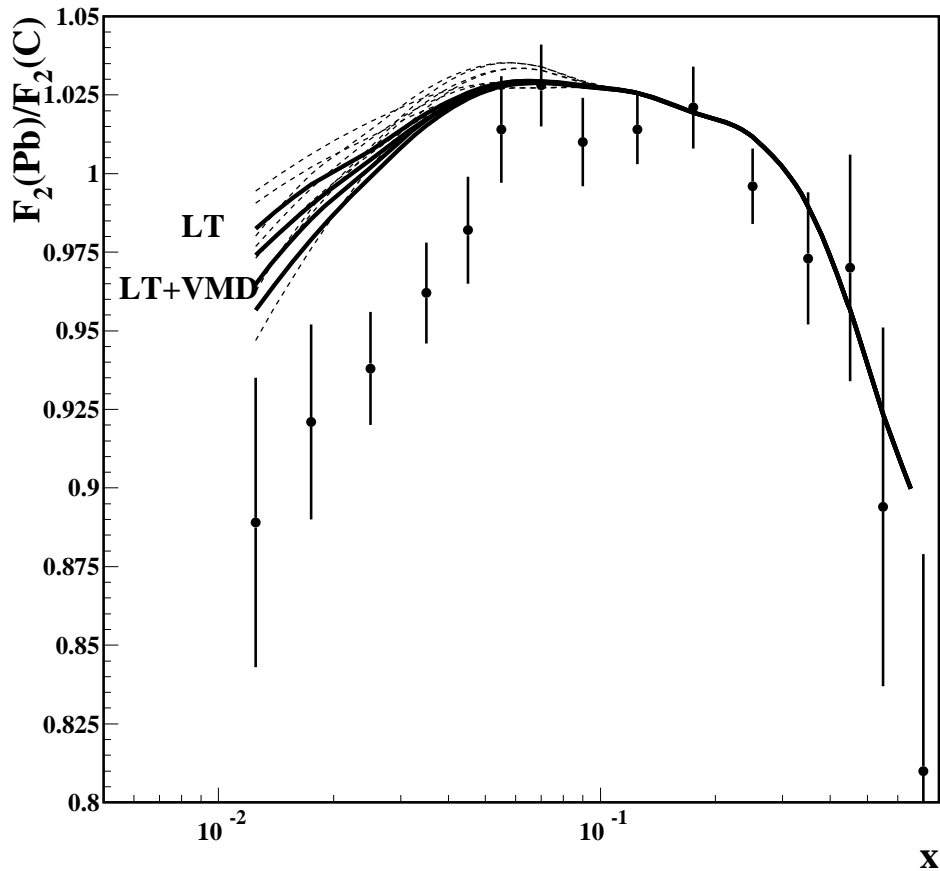


FIG. 12: Comparison of the leading twist theory results (upper set of solid curves and associated dashed error bands) to the NMC data on F_2^{Pb}/F_2^C [45]. The lower set of the solid curves is obtained by adding the VMD contribution using Eq. (18).

the contribution of small diffractive masses M_X becomes important. Production of small diffractive masses M_X is dominated by the production of vector mesons, which is definitely a higher twist phenomenon. In this kinematics, the leading twist H1 parameterization of diffraction [29] underestimates by approximately factor two the diffractive cross section as illustrated by the following estimate.

Using the definition of the diffractive differential cross section in terms of the diffractive structure function $F_2^{D(3)}$ [28] and the relation between the differential cross section on the lepton level to the total cross section on the virtual photon level (the Hund convention for

the virtual photon flux), $\sigma(\gamma^*p \rightarrow Xp)$, the latter can be written as

$$\sigma(\gamma^*p \rightarrow Xp) = \frac{4\pi^2\alpha_{e.m.}}{Q^2} \int_x^{x_{\mathbb{P},0}} dx_{\mathbb{P}} F_2^{D(3)}(\beta, Q^2, x_{\mathbb{P}}). \quad (17)$$

Then, if we restrict the integration in Eq. (17) by low diffractive masses M_X , $M_X \leq 1$ GeV, the resulting $\sigma(\gamma^*p \rightarrow Xp)$ can be compared to the cross section of electroproduction of vector mesons (dominated by the ρ meson). For instance, a comparison to the HERMES data on exclusive leptonproduction of ρ^0 mesons from hydrogen [46] at low Q^2 and W , $\langle Q^2 \rangle = 0.83$ GeV² and $\langle W \rangle = 5.4$ GeV, demonstrates that the calculation using Eq. (17) (with the restriction $M_X \leq 1$ GeV) gives only 40% of the experimental value $\sigma(\gamma^*p \rightarrow \rho^0p) = 2.04 \pm 0.10 \pm 0.43$ μb . This observation means that, in the considered case, there is no duality between the continuum and resonance contributions to low-mass inclusive diffraction.

In order to quantitatively study our conclusion about the significant role of the higher twist contribution to nuclear shadowing, we explicitly add the contribution of ρ , ϕ and ω vector mesons to our leading twist predictions in the spirit of the vector meson dominance (VMD) model. However, since about 50% of the vector meson contribution is already contained in the parameterization of inclusive diffraction, we weigh the contribution of the vector mesons to nuclear shadowing by the factor 1/2 (this enables us not to double-count the vector meson contribution). Therefore, the VMD contribution to the shadowing correction to the structure function F_2^A reads [10, 13]

$$\begin{aligned} \frac{\delta F_{2A}^{VMD}}{AF_2^N} &= -\frac{1}{2} \frac{A-1}{2} \frac{Q^2(1-x)}{\pi F_2^N} \sum_{V=\rho,\phi,\omega} \frac{\sigma_V^2(Q^2)}{f_V^2} \left(\frac{m_V^2}{Q^2 + m_V^2} \right)^2 \\ &\times \int d^2b \int_{-\infty}^{\infty} dz_1 \int_{z_1}^{\infty} dz_2 \rho_A(b, z_1) \rho_A(b, z_2) \cos(\Delta_V(z_2 - z_1)) e^{-(A/2)\sigma_V \int_{z_1}^{z_2} dz \rho_A(b, z)}, \quad (18) \end{aligned}$$

where $\Delta_V = x m_V(1 + m_V^2/Q^2)$. The VMD parameters σ_V and g_V assume their usual values [13]. For the nucleon structure function F_2^N for low Q^2 and x , we used the NMC parameterization [47] for $x > 0.006$ and the ALLM fit [48] for $x < 0.006$. In addition, since the values of Q^2 , where expression (18) is used can be as large as 10 GeV², we take into account the effect of the vector meson size decrease by introducing the explicit Q^2 dependence of σ_V : σ_V decreases by the factor of 4 when Q^2 increases from 0.6 – 0.7 GeV² to 10 GeV² [49].

The inclusion of the VMD contribution to the shadowing correction dramatically improves the agreement between our calculations and the NMC data for the considered cases of ¹²C

and ^{40}Ca , see the lower set of the solid curves in Figs. 10 and 11. This supports our conclusion about the 50% contribution of higher twist effects to nuclear shadowing in the fixed-target nuclear DIS kinematics.

As seen from Fig. 12, the inclusion of the VMD contribution does not significantly improve the agreement between our calculations and the data. Since the data points have rather large Q^2 , $Q^2 \geq 3.4 \text{ GeV}^2$, it is natural that the contribution of the ρ , ω and ϕ mesons is rather small.

At the same time, the amount of shadowing is sensitive to the diffractive masses up to $Q \sim 1.7 \text{ GeV}$, where an enhancement is also possible as compared to the leading twist fit that we employ. One has to emphasize that one is dealing here with $x_P > 0.01$, where the Pomeron component of the diffractive PDFs is known to underestimate the data by a large factor, for the recent discussion see [37]. This contribution is usually referred to as the Reggeon contribution to diffractive PDFs. However, uncertainties in the theoretical treatment of this contribution are very large due to possible interference between the Pomeron and Reggeon contribution, unreliable parameter η for the Reggeon contribution, difficulty to reliably extract the Reggeon contribution from the diffractive data. Hence we were forced to neglect this contribution in our numerical analysis. Therefore, the theoretical uncertainty due to the Reggeon contribution for $x > 0.01$ is almost out of control and, hence, our calculation for $x > 0.01$ become much less reliable. We refer the reader to Appendix B where we examine the Reggeon contribution and its influence of our predictions of nuclear shadowing and on the comparison of our results to the NMC nuclear DIS data. The domain, where the presented leading twist model is best justified, is $x < 5 \times 10^{-3}$ and $Q^2 \geq 4 \text{ GeV}^2$.

It is worth emphasizing here that our conclusion about the importance of the higher twist (HT) effects relies on the existing parameterizations of the leading twist (LT) diffractive PDFs which exclude from the fits the region of small diffractive masses. Hence the large β region is, to the large extent, an extrapolation of lower β data or effectively due to backward evolution of large β and high Q^2 data, which is rather not stable. So one cannot a priori exclude that there exists a LT parameterization which satisfies a local duality requirement in the large β , low Q^2 region. An investigation of such a possibility would require studying diffraction at lower energies than presently accessible at HERA.

One can also study the A -dependence of nuclear shadowing. Figure 13 presents a comparison of the NMC data on F_2^A/F_2^C [44, 45] to our model calculations. All data points

correspond to $x = 0.0125$; the F_2^D/F_2^C data point has $Q^2 = 2.3 \text{ GeV}^2$ and all other data points have $Q^2 = 3.4 \text{ GeV}^2$. The solid curve is our main prediction, which is obtained as a sum of the leading twist shadowing and the VMD contribution evaluated using Eq. (18). The dashed curve is obtained by increasing the nuclear shadowing correction of the solid curve by the factor two.

As seen from Fig. 13, our calculation reproduces fairly well the A -dependence of nuclear shadowing. However, as was discussed previously in connection with Fig. 12, even with the higher twist VMD contribution included, our calculation systematically underestimates the absolute value of the shadowing effect. For the heavier nuclei, we should have had a 2-3 times larger nuclear shadowing, as indicated by the dashed curve. The reason for the discrepancy between our calculations and the data is a significant Reggeon contribution to hard diffraction at $x = 0.0125$, which we neglect in our calculation. Because of this, the theoretical uncertainty of our results becomes very large for $x > 0.01$.

The leading twist model of nuclear shadowing works best in the kinematics where the VMD and Reggeon contributions to hard diffraction are small corrections and where the data on hard diffraction at HERA were taken, i.e. for $Q^2 \geq 4.5 \text{ GeV}^2$ and $x \leq 5 \times 10^{-3}$. An example of the proper application of the leading twist model of nuclear shadowing is presented in Fig. 14, which depicts the A -dependence of $F_2^A/(AF_2^N)$ at $Q^2 = 4 \text{ GeV}^2$ for $x = 10^{-3}$ (solid curve), $x = 10^{-4}$ (dashed curve) and $x = 10^{-5}$ (dot-dashed curve).

Our conclusion about the importance of the higher twist effects at small x and small Q^2 in the fixed-target data is in a broad agreement with phenomenological approaches to nuclear shadowing, which include both the scaling (leading twist) and lowest mass (ρ , ω and ϕ) vector meson (higher twist) contributions. (The only possible way to avoid such a conclusion would be the local duality scenario which we discussed earlier in this section.) In [12], the scaling contribution arises as the effect of the diffractive scattering, quite similarly in the spirit to the present work. However, it is difficult to assess the comparability of the pre-HERA parameterization of diffraction used in [12] with the modern HERA data on hard diffraction. More importantly, the effect of nuclear shadowing was discussed for the nuclear structure function F_2 and not for nPDFs (this comment also applies to all other work mentioned below). In other approaches, the scaling contribution results from the $q\bar{q}$ continuum of the virtual photon wave function [13], or from the contributions of higher mass vector mesons [15, 16], or from the aligned $q\bar{q}$ jets [11, 17], or from the asymmetric

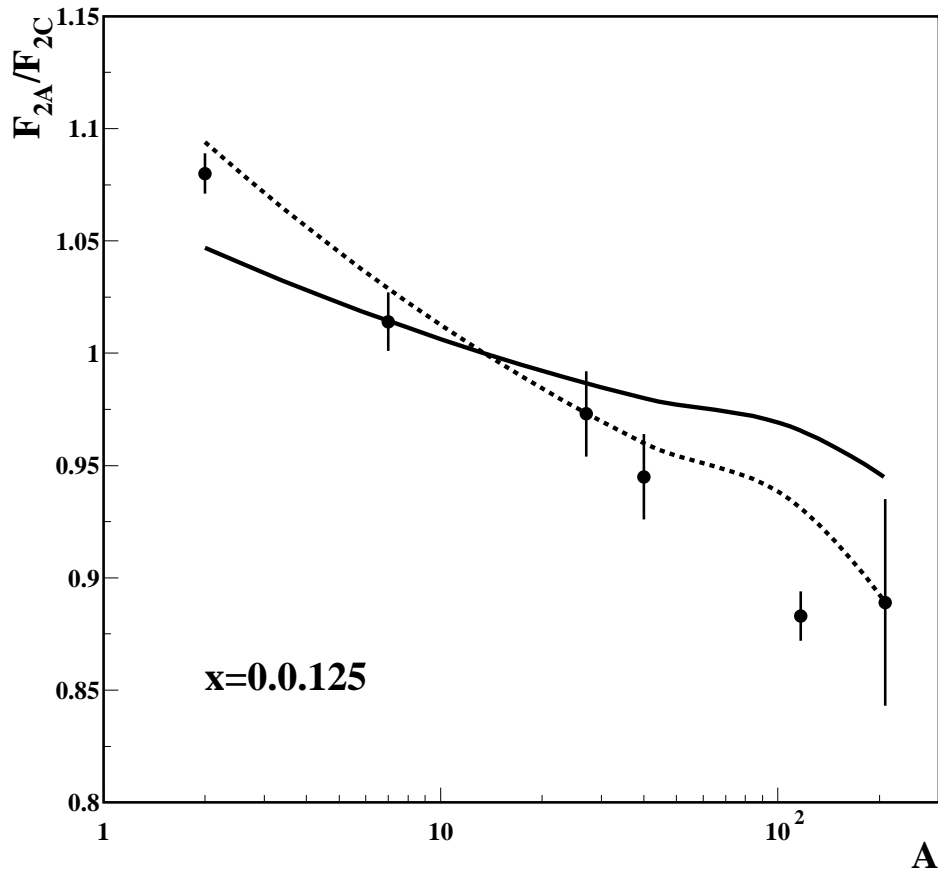


FIG. 13: A -dependence of nuclear shadowing. The NMC data on F_2^A/F_2^C [44, 45] are compared to our LT+VDM predictions (solid curve). The dashed curve is obtained by scaling up the shadowing correction of the solid curve by the factor two.

$q\bar{q}$ fluctuations of the virtual photon [18]. Note also that in the case of the real photon interaction with nuclei (the accurate data on the real photon diffraction for the relevant energies is available, see [50]), the shadowing data agree well with the Gribov's theory, see the discussion in Ref. [14].

We would like to point out that a fairly good description of the NMC data was achieved in [21], which uses the approach to nuclear shadowing based on its relation to diffraction on the nucleon. As an input for the their calculation, the authors used the phenomenological parameterizations of the inclusive and diffractive structure functions of the nucleon, which fit well the inclusive and diffractive data. However, in contrast to our strictly leading twist

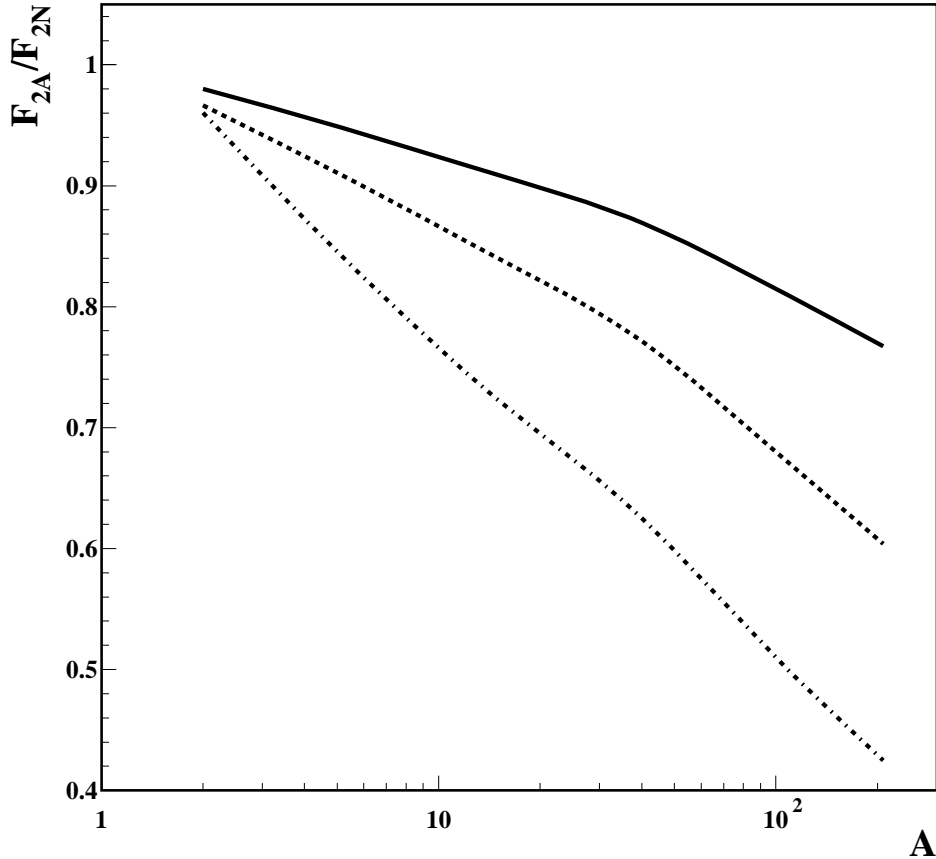


FIG. 14: The A -dependence of nuclear shadowing at $Q^2 = 4 \text{ GeV}^2$. The solid curve corresponds to $x = 10^{-3}$; the dashed curve corresponds to $x = 10^{-4}$; the dot-dashed curve corresponds to $x = 10^{-5}$.

analysis, the phenomenological parameterizations of [21] have the Q^2 -dependence of the form $(Q^2/(Q^2 + a))^b$, where a and b are numerical parameters. Hence, the analysis of [21] effectively includes higher twist contributions, which indirectly confirms our conclusion that a good description of the NMC data [44, 45] is impossible to achieve without the inclusion of the higher twist effects (contribution of vector mesons).

In addition, we would like to point to other important difference between the present analysis and the analysis of [21]. In order to evaluate nuclear shadowing as a function of Q^2 , the authors of [21] apply an equation similar in the spirit to our Eq. (14) at all Q^2 . As we explain in the end of Sect. II, the application of Eq. (14) at large Q^2 violates QCD evolution

because one then ignores the proper increase of the fluctuations of σ_{eff}^j as a result of the QCD evolution. Also, neglecting proper QCD evolution, one neglects the contribution of larger x effects – antishadowing and EMC effects – to the small- x region. The second major difference is that the use of the QCD factorization theorem for hard diffraction allowed us to make predictions for nPDFs. Since this factorization theorem is not used in [21], only nuclear structure function F_2^A is considered. Finally, the well-understood and important effect of the decrease of the coherence length with the increase of x , i.e. the factor $e^{ix_{\mathbb{P}m_N}(z_1-z_2)}$, was ignored in [21].

Next we discuss the importance of the next-to-leading order (NLO) effects in the nuclear structure function F_2 . Using the LO parameterization for the ratios of the nuclear to proton PDFs of Eskola *et al.* [1] at the initial scale $Q_0 = 1.5$ GeV, we perform QCD evolution to $Q^2 = 10$ GeV² both with NLO and LO accuracy. The resulting $F_2^{Ca}/(AF_2^N)$ ratios after the NLO evolution (dashed curve) and LO evolution (dot-dashed curve) are presented in Fig. 15. For the proton PDFs, we use CTEQ5 parameterizations [42]: CTEQ5M for the NLO calculations and CTEQ5L for the LO calculations. For comparison, we also present $F_2^{Ca}/(AF_2^N)$ (solid curves and the associated error bands) calculated using our leading twist model. The two solid curves correspond to the two scenarios of nuclear shadowing for gluons (two models for B_g). A significant difference between the solid and dashed curves in Fig. 15 demonstrates that the effects associated with the NLO QCD evolution and NLO expression for the structure function F_2 are important both in the very low- x region and in the x -region of the fixed-target data, $x > 0.003$. This gives us another indication that the LO fits to the fixed-target data of [1, 2, 3] must have significant intrinsic uncertainties, especially at low- x , where there is no data and the fits are extrapolations. In addition, Fig. 15 demonstrates that it is not self-consistent to use the LO fits for nPDFs in the NLO calculations of various hard processes with nuclei, which require NLO nPDFs as an input.

VI. EXTRACTION OF THE NEUTRON F_{2n}

The determination of the small- x behavior of the valence quark distributions relies heavily on the use of the F_2^D and F_{2p} data for the determination of the $F_{2p} - F_{2n}$ difference. The main problem is that at $x \leq 0.03$, the difference is comparable or even smaller than the nuclear shadowing correction for the deuteron, which we denote as $\delta(x, Q^2)$, $\delta(x, Q^2) \equiv$

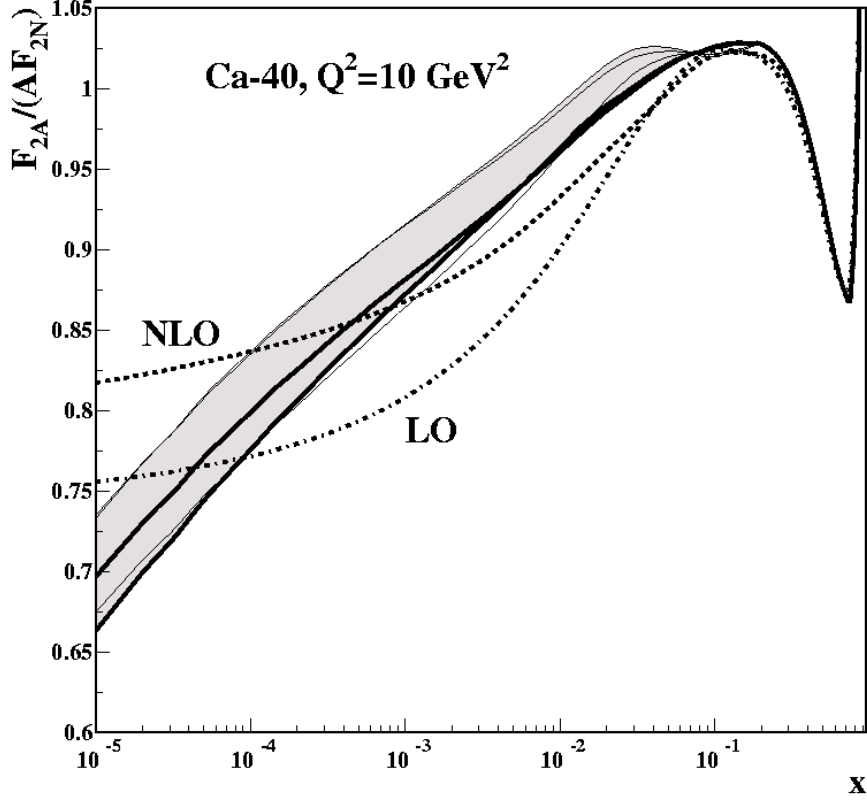


FIG. 15: LO vs. NLO evolution. The LO fits for nuclear PDFs of Eskola *et al.* [1] are evolved to $Q^2 = 10 \text{ GeV}^2$ to LO (dot-dashed curve) and to NLO (dashed curve) accuracy. Our leading twist nuclear shadowing predictions are given by the solid curves and the associated error bands.

$1 - F_2^D(x, Q^2)/(F_{2p}(x, Q^2) + F_{2n}(x, Q^2))$. Then the $F_{2p} - F_{2n}$ difference reads

$$F_{2p}(x, Q^2) - F_{2n}(x, Q^2) = 2F_{2p}(x, Q^2) - F_2^D(x, Q^2) (1 + \delta(x, Q^2)) . \quad (19)$$

In view of the discussed uncertainties in the model of diffraction (higher twist effects, subleading contributions) in the kinematics, where the NMC took their most accurate data for $\mu - D$ and $\mu - p$ scattering, one can hardly use the Gribov theory to calculate reliably $\delta(x, Q^2)$.

However, the same mechanism works both for the deuteron and for heavier nuclei as strongly suggested by Fig. 13. Hence we can employ the information on the F_2^A/F_2^D ratios in order to determine the value of $\delta(x, Q^2)$. Combining the results of the present analysis with the results of our analysis of nuclear shadowing corrections to the deuteron F_2^D [51],

we find that

$$\frac{1}{7} \left(1 - \frac{F_2^C(x, Q^2)}{F_2^D(x, Q^2)} \right) \approx 1 - \frac{F_2^D(x, Q^2)}{F_{2p}(x, Q^2) + F_{2n}(x, Q^2)}. \quad (20)$$

Using this equation and the NMC nuclear data, we find that $\delta(0.0125, 2.3 \text{ GeV}^2) \approx 0.011 \pm 0.001$. Using the CTEQ5L fit to the nucleon PDFs [42], we observe that for this kinematics nuclear shadowing significantly changes the $F_{2p}(x, Q^2) - F_{2n}(x, Q^2)$ difference

$$\frac{F_{2p}(x, Q^2) - F_{2n}(x, Q^2)}{F_{2p}(x, Q^2) - \tilde{F}_{2n}(x, Q^2)} = -\delta \frac{1+R}{1-R} = -0.63 \pm 0.06, \quad (21)$$

where $R = \tilde{F}_{2n}/F_{2p}$; \tilde{F}_{2n} is the neutron structure function extracted from the deuteron F_2^D ignoring the shadowing correction. In this estimate, we included only errors due to the experimental uncertainty in the F_2^C/F_2^D ratio.

VII. CONCLUSION AND DISCUSSIONS

The main results of this paper can be summarized as follows:

- We explain the derivation of the leading twist theory of nuclear shadowing in DIS on nuclei that relates nuclear shadowing in DIS on nuclei to DIS diffraction on the proton. The theory enables us to predict nuclear shadowing for individual nuclear PDFs in a model-independent way at small x , $10^{-5} \lesssim x \lesssim 10^{-2}$. At larger x , other nuclear effects (antishadowing, EMC effect) and details of the mechanism of diffraction at high $x_{\mathbb{P}}$ introduce a large model dependence and uncertainty.
- Nuclear shadowing corrections to nPDFs are found to be large. In particular, we predict larger shadowing than given by the fits by Eskola *et al.* [1] for gluons for all x and for quarks for $x < 5 \times 10^{-4}$. In a stark disagreement with all other approaches, we predict larger nuclear shadowing for gluons than for quarks.
- The presented formalism is applied to evaluate nuclear shadowing for nPDFs at all impact parameters. As one decreases the impact parameter, the effect of nuclear shadowing increases.
- The results of our purely leading twist calculations for the F_2^C/F_2^N , F_2^{Ca}/F_2^N and F_2^{Pb}/F_2^C ratios disagree with the corresponding fixed-target NMC data [44, 45] at low x and low Q^2 . While we cannot compare our prediction directly to the data at the

Q^2 values of the first five data points, we notice that the backwards QCD evolution is small and it does not seem to increase nuclear shadowing. Hence, we conclude that the NMC data with $Q^2 < 4 \text{ GeV}^2$ are likely to contain a significant amount (about 50%) of higher twist effects. This is supported by the explicit inclusion of the ρ , ω and ϕ meson contributions to the shadowing correction in the spirit of the vector meson dominance model. An alternative scenario would be the existence of a local duality pattern for diffraction at $x_P > 0.01$ where so far no data were taken, see Appendix B. This implies that a leading twist QCD analysis of the low- x and low- Q^2 fixed-target data will not produce reliable results for the low- x nuclear PDFs.

- Using general features of the Gribov theory and the data on $A > 2$ nuclei, it is possible to develop a reliable procedure for the extraction of the neutron F_{2n} in the NMC small- x kinematics.
- Our predictions for nPDFs, impact parameter-dependent nPDFs and the structure function F_2^A for the nuclei of ^{12}C , ^{40}Ca , ^{110}Pd , ^{197}Au and ^{206}Pb and for the kinematic range $10^{-5} \leq x \leq 1$ and $4 \leq Q^2 \leq 10,000 \text{ GeV}^2$ have been tabulated. They are available in the form of a simple Fortran program from V. Guzey upon request, vadim.guzey@tp2.rub.de. The QCD evolution was carried out using the QCDNUM evolution package [52].

We must mention that there is a renewed interest in nuclear shadowing because of the recent surprising measurements of the suppression of production of hadrons with high p_t in deuteron-gold collisions at RHIC. It was claimed that the observed suppression is a spectacular confirmation of the Colored Glass Condensate model. However, in the RHIC kinematics nPDFs are probed at relatively large values of Bjorken x , on average $x > 0.01$, which is beyond the domain of the Colored Glass Condensate model. Since leading twist nuclear shadowing is rather weak for $x > 0.01$, nuclear shadowing cannot be responsible for the dramatic effect of the suppression of the hadron spectra at forward rapidities at RHIC, see [53]. However, shadowing in the forward RHIC kinematics can be observed by selecting appropriate two jet production kinematics.

After the first version of this paper was released, there appeared an analysis [54] which calculates higher twist effects in shadowing. Similarly to us, the authors come to the conclusion that the higher twist effects in the fixed-target kinematics are large. Within uncertainties of

Nucleus	ρ_0 (fm ⁻³)	c (fm)
⁴⁰ Ca	0.0039769	3.6663
¹¹⁰ Pd	0.0014458	5.308
¹⁹⁷ Au	0.000808	6.516
²⁰⁶ Pb	0.0007720	6.6178

TABLE I: The parameters entering the nuclear one-body density $\rho_A(r)$.

their analysis, the higher twist effects could be even responsible for all shadowing observed at fixed target energies. So far the connection of the approach of [54] to the Gribov theory is not clear. In particular, the diagrams, which correspond to vector meson production (which dominates the higher twist small x contribution in the Gribov theory, see discussion in Sect. V) seem to be neglected as a very high twist effect.

Acknowledgments

This work was supported by the German-Israel Foundation (GIF), Sofia Kovalevskaya Program of the Alexander von Humboldt Foundation (Germany) and the Department of Energy (USA). V.G. is grateful to Ingo Bojak for his help and explanations of QCDNUM. We also thank H. Abramowicz for the discussion of the recent ZEUS diffractive data, and J. Morfin for emphasizing the need for a more reliable procedure for the extraction of $F_{2n}(x, Q^2)$ at small x .

APPENDIX A: NUCLEAR DENSITY ρ_A

The nuclear density ρ_A , which enters the calculation of nuclear shadowing in Eq. (14), was parametrized in a two-parameter Fermi form for ⁴⁰Ca, ¹¹⁰Pd, ¹⁹⁷Au and ²⁰⁶Pb [55]

$$\rho_A(r) = \frac{\rho_0}{1 + \exp[(r - c)/a]}, \quad (\text{A1})$$

where $r = \sqrt{|\vec{b}|^2 + z^2}$ and $a = 0.545$ fm and the parameters ρ_0 and c are presented in Table I. Also note that $\rho_A(\vec{b}, z)$ was normalized as $2\pi \int_0^\infty d|\vec{b}| \int_{-\infty}^\infty dz |\vec{b}| \rho_A(\vec{b}, z) = 1$.

For ¹²C, we used

$$\rho_A(r) = \rho_0 \left(1 + \alpha \left(\frac{r}{a} \right)^2 \right) e^{-r^2/a^2} \quad (\text{A2})$$

with $\rho_0 = 0.0132$, $\alpha = 1.403$ and $a = 1.635$ fm.

APPENDIX B: SUBLEADING (REGGEON) CONTRIBUTION TO NUCLEAR SHADOWING

The analysis of the 1994 H1 data on hard diffraction was carried out with the assumption that the diffractive structure function $F_2^{D(3)}$ is described by a sum of the effective Pomeron (leading) and Reggeon (subleading) contributions [28]

$$F_2^{D(3)}(x_{\mathcal{P}}, \beta, Q^2) = f_{\mathcal{P}/p}(x_{\mathcal{P}}) F_2^{\mathcal{P}}(\beta, Q^2) + f_{\mathcal{R}/p}(x_{\mathcal{P}}) F_2^{\mathcal{R}}(\beta, Q^2), \quad (\text{B1})$$

where $f_{\mathcal{P}/p}$ and $f_{\mathcal{R}/p}$ are the so-called Pomeron and Reggeon fluxes; $F_2^{\mathcal{P}}$ and $F_2^{\mathcal{R}}$ are the Pomeron and Reggeon structure functions. It is important to note that the both terms in Eq. (B1) are leading twist contributions. In our analysis we use fit 3 of model B of [28] which assumed no interference between the leading and subleading contributions. The latter contribution becomes important only for large values of measured $x_{\mathcal{P}}$, $x_{\mathcal{P}} > 0.01$.

In the H1 QCD analysis, $F_2^{\mathcal{R}}$ was assumed to be the pion F_2^π [56] multiplied by a free coefficient $C_{\mathcal{R}}$ to be determined from the data. Unfortunately, the value of $C_{\mathcal{R}}$ is not given in the H1 publication. Therefore, using Eq. (B1) we performed a χ^2 fit to a set of selected H1 data points with $x_{\mathcal{P}} > 0.01$ and found that $C_{\mathcal{R}} \approx 17$.

The Reggeon contribution to the nuclear shadowing correction to the F_2^A structure function has the form similar to our master equation (14)

$$\begin{aligned} \delta F_2^{A(\mathcal{R})}(x, Q^2) = & \frac{A(A-1)}{2} 16\pi C_{\mathcal{R}} \mathcal{R}e \left[\frac{(1 - i\eta_{\mathcal{R}})^2}{1 + \eta_{\mathcal{R}}^2} \int d^2b \int_{-\infty}^{\infty} dz_1 \int_{z_1}^{\infty} dz_2 \int_x^{0.1} dx_{\mathcal{P}} \right. \\ & \left. \times F_2^\pi(\beta, Q^2) \rho_A(b, z_1) \rho_A(b, z_2) e^{ix_{\mathcal{P}} m_N (z_1 - z_2)} e^{-(A/2)(1 - i\eta_{\mathcal{R}}) \sigma_{\text{eff}}^{\mathcal{R}} \int_{z_1}^{z_2} dz \rho_A(b, z)} \right]. \end{aligned} \quad (\text{B2})$$

In this equation, the $\sigma_{\text{eff}}^{\mathcal{R}}$ rescattering cross section is defined as (compare to Eq. (4))

$$\sigma_{\text{eff}}^{\mathcal{R}}(x, Q^2) = \frac{16\pi C_{\mathcal{R}}}{F_2^N(x, Q^2)(1 + \eta_{\mathcal{R}}^2)} \int_x^{0.1} dx_{\mathcal{P}} F_2^\pi(\beta, Q^2), \quad (\text{B3})$$

where it is worth noting the absence of the Reggeon flux since $f_{\mathcal{R}/p}(x_{\mathcal{P}}, t = 0) = 1$ [28].

The theoretical uncertainty associated with the Reggeon contribution originates from the uncertainty in the choice of $\eta_{\mathcal{R}}$, which is the ratio of the real to imaginary parts of the subleading exchange amplitude,

$$\eta_{\mathcal{R}} = -\frac{\xi + \cos \pi \alpha_{\mathcal{R}}(0)}{\sin \pi \alpha_{\mathcal{R}}(0)}, \quad (\text{B4})$$

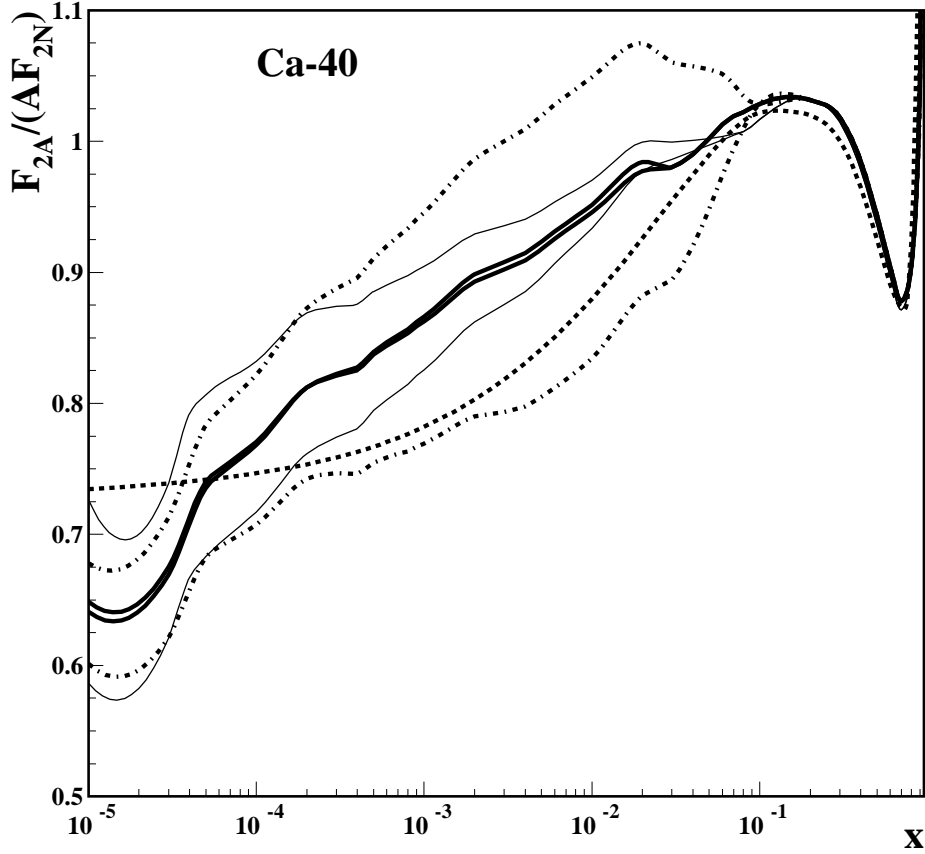


FIG. 16: The $F_2^A/(AF_2^N)$ ratio at $Q^2 = 4 \text{ GeV}^2$ for Ca-40. The thick solid curves present our main result; the thin solid curves present the uncertainty of our predictions; the dashed curve presents the fit of [1]; the dot-dashed curves is the result of the calculation including both the Pomeron and Reggeon contributions to diffraction. The lower dot-dashed curve corresponds to $\eta_R = -1$; the upper one corresponds to $\eta_R = 1$.

where $\xi = \pm 1$ is the signature factor. The intercept of the Reggeon trajectory, $\alpha_R(0)$, was a fit parameter in the H1 analysis. The fit to the H1 diffractive data gives $\alpha_R(0) = 0.5 \pm 0.11(\text{stat.}) \pm 0.11(\text{sys.})$ [28], which leads to $\eta_R = \pm 1$ depending on the signature factor. For the ρ and ω meson exchanges, $\eta_R = 1$; for the a and f meson exchanges, $\eta_R = -1$. Since no attempt was made to separate the contributions with different signatures to the Reggeon contribution in the analysis of [28] (inclusive diffraction is not sensitive to the signature of the exchange) the value of η_R is uncertain, $-1 \leq \eta_R \leq 1$.

Because of the large $|\eta_R|$, the uncertainty in the choice of η_R leads to a very significant uncertainty in the resulting shadowing correction. This is illustrated in Fig. 16 presenting $F_2^A/(AF_2^N)$ for Ca-40 at $Q^2 = 4 \text{ GeV}^2$. In Fig. 16, the thick solid curves present the predictions of our model neglecting the subleading exchange contribution to hard diffraction; the thin solid curves present the uncertainty of the predictions; the dashed curve presents the result of [1]; the dot-dashed curves is the result of the calculation including both the Pomeron and Reggeon contributions to diffraction. The lower dot-dashed curve corresponds to $\eta_R = -1$; the upper one corresponds to $\eta_R = 1$. As seen from Fig. 16, the variation of η_R between its lower and upper limits leads to a dramatic change in the predicted nuclear shadowing.

The influence of the Reggeon contribution on the comparison of our predictions to the NMC fixed-target nuclear DIS data is presented in Figs. 17 and 18. The upper set of solid curves and the associated dashed error bands is the result of the calculation using only the Pomeron contribution to diffraction. The lower set of the solid curves is obtained by adding the VMD contribution using Eq. (18). The dot-dashed curves are the results of the calculation taking into account the Pomeron, Reggeon and VMD contributions. The lower dot-dashed curve corresponds to $\eta_R = -1$; the upper one corresponds to $\eta_R = 1$.

As seen from Figs. 17 and 18, varying η_R in the $-1 \leq \eta_R \leq 1$ range, one obtains a wide spectrum of predictions for F_2^{Ca}/F_2^D and F_2^{Pb}/F_2^C , which accommodate the NMC data. This indicates the possibility of a duality between the higher twist vector meson contribution and the leading twist subleading contribution.

-
- [1] K.J. Eskola, V.J. Kolhinen and P.V. Ruuskanen, Nucl. Phys. B **535** (1998) 351; K.J. Eskola, V.J. Kolhinen and C.A. Salgado, Eur. Phys. J. C **9**, 61 (1999).
 - [2] M. Hirai, S. Kumano and M. Miyama, Phys. Rev. D **64**, 034003 (2001); M. Hirai, S. Kumano and T.-H. Nagai, Phys. Rev. C **70**, 044905 (2004).
 - [3] S. Li and X.N. Wang, Phys. Lett. B **527**, 85 (2002).
 - [4] For a recent comparison of fits of Ref. [1] and [2], see K.J. Eskola, H. Honkanen, V.J. Kolhinen and C.A. Salgado, hep-ph/0302170.
 - [5] D. de Florian and R. Sassot, Phys. Rev. D **69**, 074028 (2004).

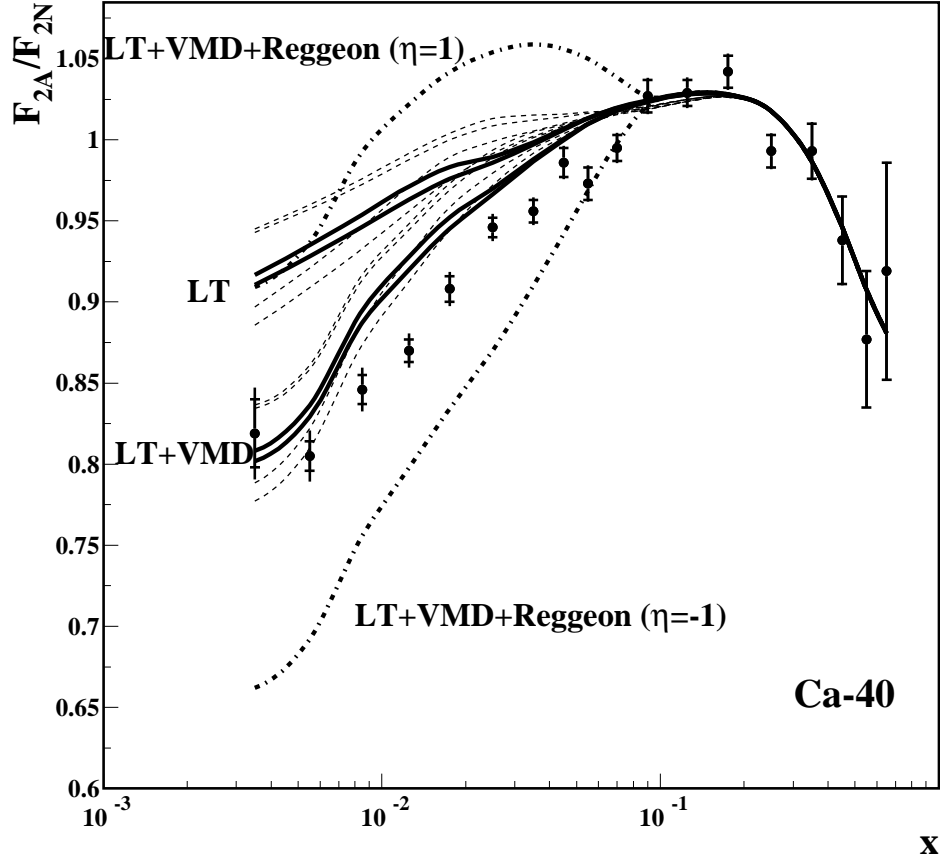


FIG. 17: Comparison of the leading twist theory results (the upper set of solid curves and associated dashed error bands) to the NMC data on F_2^{Ca}/F_2^N [44]. The lower set of the solid curves is obtained by adding the VMD contribution using Eq. (18). The dot-dashed curves are the sums of the Pomeron, Reggeon and VMD contributions. The lower dot-dashed curve corresponds to $\eta_R = -1$; the upper one corresponds to $\eta_R = 1$.

- [6] V.N. Gribov, Sov. Phys. JETP **29**, 483 (1969) [Zh. Eksp. Teor. Fiz. **56**, 892 (1969)].
- [7] J.C. Collins, Phys. Rev. D **57**, 3051 (1998); Erratum *ibid* **61**, 019902 (1999).
- [8] L. Frankfurt and M. Strikman, Eur. Phys. J. A **5**, 293 (1999).
- [9] L. Frankfurt, V. Guzey, M. McDermott and M. Strikman, JHEP **0202**, 27 (2002).
- [10] T.H. Bauer, R.D. Spital, D.R. Yennie and F.M. Pipkin, Rev. Mod. Phys. **50**, 261 (1978).
- [11] L. Frankfurt and M. Strikman, Phys. Rept. **160**, 235 (1988).
- [12] W. Melnitchouk and A.W. Thomas, Phys. Rev. D **47**, 3783 (1993); Phys. Lett. B **317**, 437

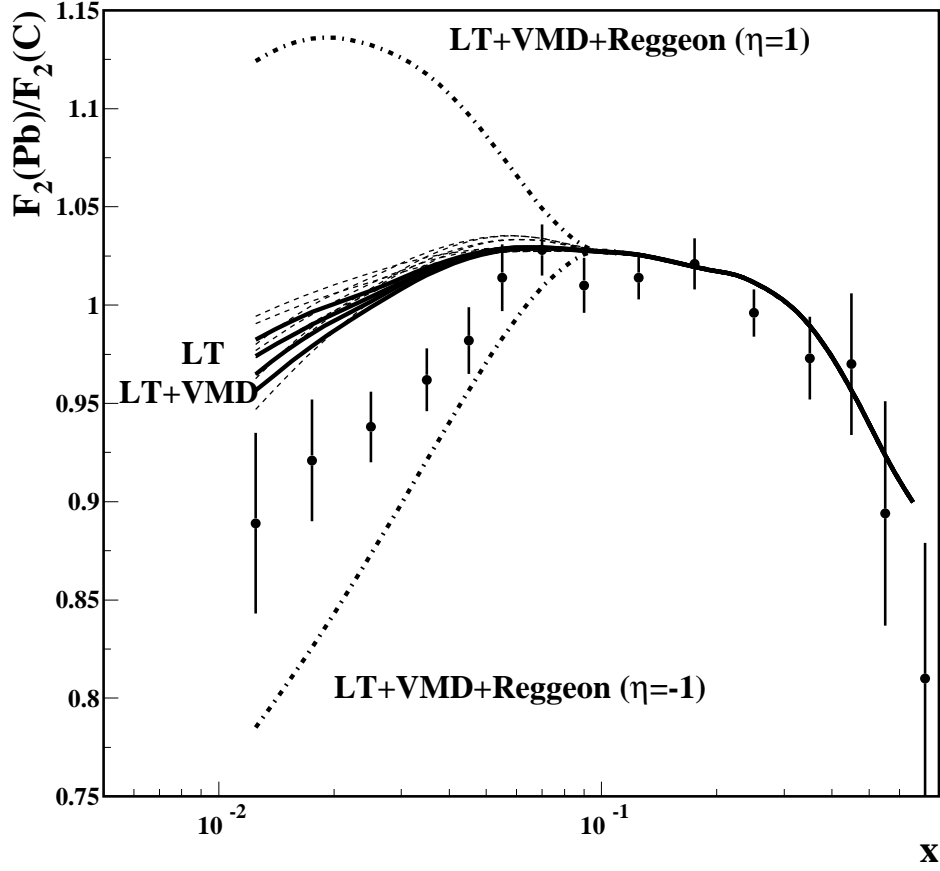


FIG. 18: Comparison of the leading twist theory results (the upper set of solid curves and associated dashed error bands) to the NMC data on F_2^{Pb}/F_2^C [45]. The lower set of the solid curves is obtained by adding the VMD contribution using Eq. (18). The dot-dashed curves are the sums of the Pomeron, Reggeon and VMD contributions. The lower dot-dashed curve corresponds to $\eta_R = -1$; the upper one corresponds to $\eta_R = 1$.

(1993); Phys. Rev. C **52**, 3373 (1995); Phys. Rev. C **67**, 038201 (2003).

[13] G. Piller, W. Ratzka and W. Weise, Z. Phys. A **352**, 427 (1995).

[14] G. Piller and W. Weise, Phys. Rept. **330**, 1 (2000).

[15] J. Kwiecinski and B. Badelek, Phys. Lett. B **208**, 508 (1988).

[16] G. Shaw, Phys. Rev. D **47**, R3676 (1993).

[17] L.L. Frankfurt and M.I. Strikman, Nucl. Phys. B **316**, 340 (1989).

[18] N.N. Nikolaev and B.G. Zakharov, Phys. Lett. B **260**, 414 (1991); Z. Phys. **49**, 607 (1991).

- [19] B. Kopeliovich and B. Povh, Phys. Lett. B **367**, 329 (1996).
- [20] S.J. Brodsky and H.J. Lu, Phys. Rev. Lett. **64**, 1342 (1990).
- [21] A. Capella, A. Kaidalov, C. Merino, D. Pertermann and J. Tran Thanh Van, Eur. Phys. J. C **5**, 111 (1998).
- [22] V.A. Abramovsky, V.N. Gribov and O.V. Kancheli, Yad. Fiz. **18**, 595 (1973) [Sov. J. Nucl. Phys. **18**, 308 (1974)].
- [23] L. Alvero, L. Frankfurt and M. Strikman, Eur. Phys. J. A **5**, 97 (1999).
- [24] R.J. Glauber, Phys. Rev. **100**, 242 (1955).
- [25] J.C. Collins, D.E. Soper and G. Sterman, Nucl. Phys. B **308**, 833 (1988).
- [26] L. Frankfurt, M. Strikman, and M. Zhalov, hep-ph/0412052.
- [27] ZEUS Collab., J. Breitweg *et al.*, Eur. Phys. J. C **6** (1999) 43.
- [28] H1 Collab., C. Adloff *et al.*, Z. Phys. C **76**, 613 (1997).
- [29] The FORTRAN code with the analysis of the 1994 H1 inclusive diffraction can be found at <http://www-h1.desy.de/h1/www/h1work/dif/h1994.html>.
- [30] H1 Collab., C. Adloff *et al.*, Eur. Phys. J. C **20**, 29 (2001).
- [31] L. Alvero, J.C. Collins, J. Terron and J.J. Whitmore, Phys. Rev. D **59**, 074022 (1999).
- [32] F. Hautmann, Z. Kunszt and D.E. Soper, Nucl. Phys. B **563**, 153 (1999).
- [33] H1 Collab., C. Adloff *et al.*, in *Proceedings of ICHEP02, Amsterdam, 2002* (Elsevier Science, New York, 2003).
- [34] ZEUS Collab., J. Breitweg *et al.*, Eur. Phys. J. C **1**, 81 (1998).
- [35] H1 Collab., C. Adloff, Phys. Lett. B **483**, 23 (2000).
- [36] ZEUS Collab., A. Bruni, in *Proceedings of DIS 2000, Liverpool, 2000*, edited by J.A. Gracey and T. Greenshaw (World Scientific, Singapore, 2000).
- [37] ZEUS Collab., S. Chekanov *et al.*, Eur. Phys. J. C **38**, 43 (2004) [hep-ex/0408009].
- [38] V.N. Gribov and A.A. Migdal, Sov. J. Nucl. Phys. **8**, 583 (1969).
- [39] G. Altarelli, R. D. Ball, and S. Forte, Nucl. Phys. B **674**, 459 (2003) [hep-ph/0306156]; M. Ciafaloni, D. Colferai, G. P. Salam and A. M. Stasto, Phys. Rev. D **68**, 114003 (2003) [hep-ph/0307188].
- [40] L. McLerran, hep-ph/0311028.
- [41] L.L. Frankfurt, M.I. Strikman and S.Liuti, Phys. Rev. Lett. **65**, 1725 (1990).
- [42] H. Lai *et al.*, Eur. Phys. J. C **12**, 375 (2000).

- [43] R. Vogt, hep-ph/0411378.
- [44] NMC Collab., P. Amaudruz *et al.*, Nucl. Phys. B **441**, 3 (1995).
- [45] NMC Collab., M. Arneodo *et al.*, Nucl. Phys. B **481**, 3 (1996).
- [46] HERMES Collab., A. Airapetian *et al.*, Eur. Phys. J. C **17**, 389 (2000).
- [47] NMC Collab., M. Arneodo *et al.*, Phys. Lett. B **364**, 107 (1995).
- [48] H. Abramowicz, E.M. Levin, A. Levy, and U. Maor, Phys. Lett. B **269**, 465 (1991).
- [49] L. Frankfurt, W. Koepf, and M. Strikman, Phys. Rev. D **54**, 3194 (1996).
- [50] T.J. Chapin *et al.*, Phys. Rev. D **31**, 17 (1985).
- [51] L. Frankfurt, V. Guzey, and M. Strikman, Phys. Rev. Lett. **91**, 202001 (2003) [hep-ph/0304149].
- [52] All the relevant information about the QCDNUM evolution program can be found at <http://www.nikhef.nl/~h24/qcdnum>.
- [53] V. Guzey, M. Strikman, and W. Vogelsand, Phys. Lett. B **603**, 173 (2004) [hep-ph/0407201].
- [54] J.-w. Qiu and I. Vitev, hep-ph/0309094.
- [55] H. De Vries, C.W. De Jager, and C. De Vries, At. Data Nucl. Data Tables **36**, 495 (1987).
- [56] J.F. Owens, Phys. Rev. D **30**, 943 (1984).
- [57] It is possible to derive the Gribov theorem including corrections due to the real part of the diffractive amplitude (those were neglected in the Gribov's original approach based on the Pomeron model with $\alpha_P(0) = 1$) using the Abramovskii, Gribov and Kancheli (AGK) cutting rules [22], see [8, 9]. Hence, in the small- x limit ($x \ll 10^{-2}$), the relation between shadowing and diffraction is essentially a consequence of unitarity.
- [58] The real part of the amplitude was neglected in [21], and, therefore, their corresponding expressions do not contain the factor $(1 - i\eta)^2/(1 + \eta^2)$.
- [59] The double rescattering term can be calculated using Eq. (2) at any Q^2 . However, the quasieikonal approximation employed in Eq. (6) is best justified at low $Q^2 \sim Q_0^2$, where fluctuations in the strength of the interaction are smaller (see the discussion in Ref. [9]). The QCD evolution equations automatically account for the proper increase of the fluctuations of the effective cross section around its average value σ_{eff}^j with an increase of Q^2 . This important effect is omitted if one attempts to apply Eq. (6) at $Q^2 > Q_0^2$ with a Q^2 -dependent $\sigma_{\text{eff}}^j(Q^2)$.